Mon. Not. R. Astron. Soc. **276,** 1067–1084 (1995)

Studies of star formation in isolated small dark clouds – II. A southern ammonia survey

T. L. Bourke,[1]★† A. R. Hyland,[1,2]†‡ G. Robinson,[1]† S. D. James[1]† and C. M. Wright[1,3]†

[1] *Department of Physics, University College, The University of New South Wales, Australian Defence Force Academy, Canberra, ACT 2600, Australia*

[2] *Faculty of Science, The University of New South Wales, Sydney, NSW 2052, Australia*

[3] *Max-Planck-Institut für extraterrestrische Physik, Postfach 1603, D-85740 Garching bei München, Germany*

Accepted 1995 April 12. Received 1995 April 7; in original form 1994 August 4

ABSTRACT

A study of the set of small, southern molecular clouds (globules) compiled by Bourke, Hyland & Robinson has been undertaken, through radio observations of ammonia using the Parkes 64-m telescope. The aim of the study is to determine the physical characteristics of the globules, their role in the formation of low-mass stars, and the physical mechanism that triggers the star formation process, or stabilizes the globules against collapse. With this general aim in mind, the (1,1) and (2,2) inversion transitions of ammonia have been surveyed in order to determine the densities, temperatures and masses of the globules.

Half of the globules have been detected in ammonia, but only 6 per cent of the detections are 'strong' ($T_a^* \geq 0.35$ K). Comparing the globule properties with those of Benson & Myers for cores within complexes, we find that the globules are less opaque and less dense, and are less active sites of star formation. Other properties are comparable. The Vela cometary globules are detected more readily in ammonia than the more isolated globules, and are more active star formation sites. These results suggest that the dense core's environment, in particular the presence of either a large external mass or a significant stellar wind, plays an important role in initiating the star formation process.

Key words: surveys – stars: formation – stars: pre-main-sequence – ISM: clouds – ISM: molecules – infrared: stars.

1 INTRODUCTION

Small molecular clouds or Bok globules (Bok & Reilly 1947) are now well-accepted as being among the sites of formation of low-mass stars. Clemens & Barvainis (1988) compiled a catalogue of 248 of these clouds located in the northern sky, and Bourke, Hyland & Robinson (1995, Paper I, hereafter BHR) have presented a complementary catalogue of 169 clouds in the southern sky. The simple structure and isolation of these clouds mean that they are ideally suited to the study of low-mass star formation, with the derivation of their physical characteristics representing an important first stage of investigation.

Several molecules, e.g. CO, NH_3, H_2CO and CS, have been used to derive information on the physical conditions within molecular clouds. Extensive CO observations (Clemens & Barvainis 1988; Clemens, Yun & Heyer 1991) have provided excellent information on the temperatures and dynamics within such clouds. However, neither ^{12}CO nor ^{13}CO traces high-density gas, and hence neither provides the data required for the identification of likely sites of low-mass star formation (Benson & Myers 1989, hereafter BM).

Ammonia, on the other hand, is an excellent tracer of high-density gas, requiring densities greater than 10^3 cm^{-3} to excite the $(J,K)=(1,1)$ rotation inversion transition to

★ Present address: Harvard–Smithsonian Center for Astrophysics, 60 Garden St, MS 42, Cambridge, MA 02138, USA.
†Email: tbourke@cfa.harvard.edu (TLB); dvc@scu.edu.au (ARH); garry@phadfa.ph.adfa.oz.au (GR); steve@phadfa.ph.adfa.oz.au (SDJ); wright@mpe-garching.mpg.de (CMW).
‡Present address: Office of the Vice Chancellor, Southern Cross University, Lismore, NSW 2480, Australia.

observable strength at the low temperatures inferred for dark molecular clouds (Ho & Townes 1983). Observations of the many hyperfine components of the (1,1) transition of ammonia enable the intrinsic linewidth, optical depth and excitation temperature of the transition to be determined. Combination of observations of the (1,1) line with those of the (2,2) line then enables the determination of the kinetic temperature and density of the cloud. Mapping of the cloud allows the core size and, when the density is known, the core mass to be determined. Ammonia is therefore an extremely versatile diagnostic probe of the conditions in dense molecular clouds.

In this paper we present the results of a complete survey of the catalogue of small molecular clouds listed in Paper I (BHR) for emission in the (1,1) transition of ammonia. There are two main thrusts to this study. The first is to survey the dark cloud sample for dense cores, and to determine the physical properties of these dense cores. The second is to compare the properties of the cores found within the small, isolated molecular clouds with those of the cores found in the larger dark cloud complexes, specifically those studied by BM in their ammonia survey. In Paper III (Bourke et al., in preparation) we will present the results of ammonia mapping of a number of the stronger sources, and their dynamical interpretation.

2 OBSERVATIONS AND SURVEY RESULTS

2.1 Observations

The ammonia observations reported here were undertaken at the Parkes radio telescope in 1990 August–September, 1991 January and November, 1992 June, 1993 March and 1994 February with a *K*-band maser receiver. A number of different bandwidths and resolutions were employed during the various sessions. For the 1990 August–September and 1991 January sessions, the Parkes 1024-channel digital correlator was split into four sections of 256 channels with a bandwidth of 5 MHz (velocity resolution $\Delta v = 0.25$ km s^{-1}). Some observations were also made in 1991 January with the correlator split into two sections of 512 channels, allowing for a higher resolution ($\Delta v = 0.12$ km s^{-1}). In 1991 November this latter setup was used exclusively. In 1992 June the new Parkes correlator was used, first with two sections of 1024 channels and a bandwidth of 8 MHz ($\Delta v = 0.10$ km s^{-1}), then with a bandwidth of 16 MHz ($\Delta v = 0.20$ km s^{-1}), and finally with two sections of 2048 channels with a bandwidth of 16 MHz ($\Delta v = 0.10$ km s^{-1}), allowing a greater velocity range to be observed. In 1993 March the bandwidth was either 8 MHz over 512 channels (new correlator) or 5 MHz over 512 channels (old correlator), providing a velocity resolution of 0.20 or 0.12 km s^{-1} respectively. Since we were mainly concerned with mapping during this session, a large velocity range was not required. Furthermore, because of problems with the new correlator we were forced to switch between the two. In 1994 February the bandwidth was 8 MHz over 2048 channels, giving $\Delta v = 0.05$ km s^{-1}.

The observations were performed in total-power mode. In most survey positions the total integration time was 60 min, consisting of alternate pairs of observations of 5 min on-source and 5 min off-source. The off-source observations were alternated between 5 min west in time (for reference spectra taken before the source spectra) and 5 min east in time (for reference spectra taken after source spectra) of the survey position, thereby minimizing the problem of elevation-dependent corrections between source and reference spectra. A quotient was formed from each pair, and the quotients averaged to produce the spectra.

System temperatures of 70–100 K were recorded in good weather. The FWHM beamsize at the observed frequencies ($\sim$23.7 GHz), θ_b, was 1.4 arcmin, and the beam efficiency, η, as determined from observations of Virgo A (see e.g. Kuiper et al. 1987), was found to be 0.32. Pointing checks indicate that the pointing accuracy was better than about 10 arcsec for all sessions. The spectra have been corrected for atmospheric attenuation and the variation of telescope gain with elevation. For the latter, a gain curve was derived for the telescope at 23.7 GHz. This was undertaken during the 1992 June session by scanning across Centaurus A at various zenith angles, and comparing the observed flux with that received from Virgo A, the latter being observed at a nearly constant zenith angle of 45°. The procedure has been described in full by Bourke (1994). Polynomials of up to order three were used to baseline the data. In most cases the spectra have been Hanning-smoothed. The rms noise in the off-line channels of the reduced spectra was typically $\sim$0.03 K or less. All data reduction was performed with the Australia Telescope National Facility (ATNF) in-house spectral line reduction package SPC.

The initial search for ammonia emission from the (1,1) transition within the complete list of dark clouds was completed in 1992 June. Observations of the (2,2) line were undertaken primarily during 1991 November and 1993 March. Mapping of the strongest sources was begun in 1991 November and essentially completed in 1993 March. Some weaker sources were partially mapped in 1994 February. Results and analysis of the mapping will be reported in Paper III.

2.2 Ammonia survey results

All 169 clouds were surveyed in at least one position (those given by BHR) for ammonia emission. Gaussians were fitted to the main line of the calibrated spectra when visible, and the results of these fits are given in Table 1. Also listed in this table is the globule B68, which does not lie south of $-33°$ declination, but which satisfies all our other selection criteria and is a strong ammonia emitter. It is included here to improve the statistics of the derived globule physical characteristics, since there are relatively few globules the properties of which could be fully determined (see Section 4 below).

In Table 1, column 1 lists the cloud number as introduced by BHR, column 2 lists the cloud name, and column 3 lists the rms noise level, which is taken as the 1σ level in the off-line channels of the spectrum. Columns 4–6 list the results of the Gaussian fit to the central component, with the uncertainties in the fit quoted in parentheses. Where no signal was visible the velocity range observed is quoted. Column 7 indicates the velocity of the signal observed in previous studies, where the superscript 1 refers to H_2CO observations of Zealey et al. (1983), 2 to H_2CO observations of Goss et al. (1980), 3 to CO observations of de Vries et al. (1984), 4 to H_2CO observations of Sandqvist & Lindroos (1976), 5 to NH_3 observations of Kuiper et al. (1987), 6 to CO observations of Clemens et al. (1991), 7 to NH_3 observations of

Table 1. Ammonia survey results.

Number	DC Name	rms (K)	T_a^* (K)	V_{lsr} [a] ($km\,s^{-1}$)	ΔV ($km\,s^{-1}$)	V_{other} [b] ($km\,s^{-1}$)	Session[c]	*IRAS* [d]
1	249.7-2.1	0.042	...	−31, 31	...	ND[1]	N91	
2	251.7+0.2	0.032	0.24 (0.02)	5.09 (0.03)	0.69 (0.07)		N91	Y
3	251.8+0.0	0.030	...	−101, 101	...		Ju92c	Y
4	251.9+0.0	0.037	...	−101, 101	...		Ju92c	
5	252.2+0.7	0.028	0.23 (0.02)	2.03 (0.02)	0.64 (0.06)		Ju92c	Y
6	252.3+0.5	0.022	...	−101, 101	...		Ju92c	
7	252.5+0.1	0.025	0.22 (0.01)	4.85 (0.02)	0.78 (0.04)	ND[1]	Ju92c	Y
8	253.1-1.7A	0.034	0.35 (0.01)	6.04 (0.02)	0.95 (0.04)	5.9[1]	N91	
9	253.1-1.7B	0.026	0.19 (0.02)	5.87 (0.03)	0.71 (0.07)		N91	
10	253.1-1.7C	0.029	0.24 (0.01)	6.32 (0.03)	1.02 (0.06)		N91	
11	253.1-1.7D	0.027	...	−25, 37	...		N91	
12	253.3-1.6	0.019	0.64 (0.05)	6.18 (0.04)	1.02 (0.09)	5.4[1] 6.0[2] 5.2[3]	Ja91a	Y
13	253.6+2.9	0.034	0.14 (0.02)	6.57 (0.04)	0.64 (0.10)	6.4[1] 6.5[2]	N91	Y
14	253.8-10.9	0.015	0.24 (0.02)	−1.04 (0.03)	0.75 (0.08)	ND[2]	Ju92b	
15	255.3-14.4	0.023	0.11 (0.02)	4.00 (0.03)	0.81 (0.08)	3.5[1] 4.1[2]	N91	Y
16	255.4-3.9	0.030	...	−101, 101	...		Ju92c	
17	256.2-14.1	0.015	0.10 (0.01)	3.47 (0.06)	1.00 (0.13)		Ju92b	Y
18	256.9+2.6	0.020	...	−101, 101	...		Ju92c	Y
19	257.2-10.3	0.024	0.09 (0.01)	−3.42 (0.06)	0.68 (0.14)		N91	Y
20	259.0-13.2	0.045	0.19 (0.03)	0.93 (0.06)	0.89 (0.14)		N91	
21	259.4-12.7	0.027	0.20 (0.02)	1.45 (0.03)	0.61 (0.06)	1.2[2,3]	N91	
22	259.5-16.4	0.024	0.12 (0.01)	3.84 (0.06)	0.98 (0.13)	4.0[1] 3.5[2,3]	N91	Y
23	259.9-0.0	0.016	0.24 (0.02)	7.68 (0.06)	1.75 (0.14)	7.5[2,3]	Ju92b	Y
24	260.0-3.8	0.020	0.07 (0.01)	−11.88 (0.06)	0.75 (0.13)		Ju92c	
25	260.7-12.4	0.032	0.17 (0.01)	−0.05 (0.03)	0.71 (0.07)	ND[2]	N91	Y
26	262.5-13.4	0.028	0.11 (0.01)	−0.88 (0.05)	0.83 (0.11)	−1.0[1]	N91	Y
27	262.9-14.7	0.032	0.19 (0.03)	−0.83 (0.04)	0.59 (0.09)	ND[1]	N91	Y
28	262.9-15.5	0.031	0.26 (0.02)	−0.73 (0.02)	0.70 (0.05)		N91	
29	264.5+5.6	0.022	...	−101, 101	...		Ju92c	
30	265.3-0.0	0.023	...	−101, 101	...	ND[4]	Ju92c	
31	265.7-7.7	0.013	0.05 (0.01)	2.87 (0.07)	0.62 (0.16)		Ju92b	Y
32	266.0+4.3	0.035	...	−31, 31	...	−1.5[2]	N91	
33	266.0-4.3	0.025	...	−101, 101	...		Ju92c	
34	267.2-7.2	0.031	0.20 (0.01)	4.95 (0.06)	0.78 (0.20)		M93b	Y
35	267.4-0.9	0.017	0.06 (0.01)	−2.70 (0.13)	0.64 (0.31)	ND[2]	A90	
36	267.4-7.5	0.015	0.39 (0.03)	5.28 (0.03)	0.96 (0.07)	5.3[3,5]	A90	Y
37	267.5-7.4	0.021	0.30 (0.02)	5.99 (0.03)	0.86 (0.08)		A90	
38	267.6-6.0A	0.017	0.18 (0.01)	5.85 (0.03)	0.78 (0.07)		Ju92b	
39	267.6-6.0B	0.028	0.10 (0.01)	5.72 (0.03)	0.39 (0.08)		Ju92c	
40	267.6-6.4	0.021	0.07 (0.01)	5.63 (0.11)	0.82 (0.26)	5.3[2]	Ja91a	
41	267.7-7.4	0.029	0.75 (0.02)	5.39 (0.01)	0.79 (0.02)	5.3[2]	N91	Y
42	267.9-7.8	0.032	0.08 (0.01)	6.21 (0.13)	1.57 (0.31)		N91	
43	269.4+3.0	0.026	0.08 (0.02)	−1.69 (0.06)	0.69 (0.14)	−2.3[2,3]	N91	
44	269.5+4.0	0.028	0.08 (0.01)	−3.24 (0.11)	0.83 (0.26)		N91	
45	269.7-3.9	0.023	...	−101, 101	...		Ju92c	
46	270.6-4.7	0.053	...	−26, 36	...	−6.7[1]	N91	
47	272.5+2.0	0.028	...	−101, 101	...		Ju92c	Y
48	273.2+2.4	0.026	...	−101, 101	...		Ju92c	
49	273.3+2.5	0.029	...	−101, 101	...		Ju92c	
50	273.8+3.2	0.027	...	−101, 101	...		Ju92c	
51	274.1+3.9	0.034	...	−101, 101	...		Ju92c	
52	274.1+2.7	0.015	0.06 (0.01)	−3.71 (0.07)	0.92 (0.16)	−3.5[2]	Ju92b	
53	274.2-0.4	0.047	0.19 (0.03)	5.70 (0.08)	0.78 (0.20)		Ja91a	
54	274.3+3.4	0.031	...	−101, 101	...		Ju92c	Y
55	275.9+1.9	0.026	0.41 (0.01)	−5.45 (0.01)	0.84 (0.03)		Ju92c	Y
56	276.2-10.6	0.018	...	−31, 31	...		A90	Y
57	285.3-1.6	0.047	...	−29, 33	...		N91	
58	289.3-2.8	0.017	0.12 (0.01)	−6.98 (0.08)	1.73 (0.20)		A90	Y
59	291.1-1.7	0.016	0.26 (0.02)	−4.52 (0.03)	0.87 (0.06)	−4.8[2,3]	A90	
60	291.4-0.2	0.032	0.15 (0.02)	−6.52 (0.13)	1.12 (0.29)	−6.5[2]	A90	

Table 1. *Continued.*

Number	DC Name	rms (K)	T_a^* (K)	V_{lsr} [a] (km s^{-1})	ΔV (km s^{-1})	V_{other} [b] (km s^{-1})	Session[c]	*IRAS* [d]
61	293.1+0.6	0.046	...	−29, 33	...		N91	
62	293.2+0.4	0.015	...	−101, 101	...		Ju92b	
63	293.3+0.1	0.022	...	−50, 50	...		Ju92a	
64	293.3-0.9	0.019	0.20 (0.02)	−27.47 (0.05)	1.29 (0.12)		A90	
65	294.3+2.7	0.024	...	−31, 31	...		N91	
66	294.3-0.1	0.021	...	−101, 101	...		Ju92c	
67	294.9+0.1	0.031	0.10 (0.01)	−10.78 (0.05)	0.56 (0.11)		Ju92c	Y
68	295.0+3.4	0.018	0.37 (0.03)	−7.55 (0.03)	0.85 (0.07)	−7.7[2,3]	Ju92b	
69	295.4+0.5	0.028	...	−101, 101	...		Ju92c	
70	295.5+0.4	0.027	...	−101, 101	...		Ju92c	
71	297.7-2.8	0.047	1.02 (0.03)	−4.45 (0.01)	1.02 (0.03)	−4.8[2]	N91	Y
72	298.3-2.8	0.028	0.07 (0.01)	−4.71 (0.08)	0.89 (0.20)		Ju92c	
73	299.6+5.6	0.012	...	−101, 101	...		Ju92b	Y
74	300.0-3.7	0.017	0.12 (0.02)	−5.78 (0.06)	0.73 (0.14)		A90	
75	300.2-3.5	0.030	...	−54, 46	...	−5.8[2]	M93a	
76	300.6-3.1	0.015	0.07 (0.01)	−5.37 (0.06)	0.65 (0.14)	−5.6[2]	Ja91a	
77	300.7-1.0	0.026	0.15 (0.02)	−5.34 (0.02)	0.44 (0.06)	−6.2[2] −6.1[3]	Ju92c	
78	301.2-0.4	0.027	0.15 (0.01)	−4.80 (0.03)	0.69 (0.07)	−5.1[3]	N91	
79	301.7-6.7	0.026	...	−101, 101	...		Ju92c	Y
80	301.7-7.2	0.029	...	−101, 101	...	ND[2]	Ju92c	
81	301.7-2.6	0.018	...	−101, 101	...		Ju92b	Y
82	302.0-7.0	0.028	0.19 (0.02)	4.76 (0.03)	0.65 (0.06)		Ju92c	
83	302.1+7.4	0.025	0.12 (0.01)	−15.12 (0.03)	0.75 (0.25)		Ju92c	Y
84	302.6-15.9	0.045	...	−36, 26	...		N91	
85	303.3+1.3	0.028	0.09 (0.02)	−3.71 (0.04)	0.52 (0.09)	−3.9[2]	N91	
86	303.8-14.2	0.075	0.89 (0.03)	3.67 (0.02)	0.83 (0.04)	3.7[2]	F94	Y
87	307.3+2.9	0.028	0.10 (0.02)	32.72 (0.05)	0.53 (0.11)		M93a	Y
88	314.8-5.1	0.019	0.06 (0.02)	−4.16 (0.11)	0.69 (0.25)	−4.5[2]	Ju92b	Y
89	315.8-27.5A	0.030	...	−71, −9	...		N91	Y
90	315.8-27.5B	0.052	0.21 (0.04)	−37.84 (0.04)	0.32 (0.10)		N91	
91	316.3+4.9	0.028	...	−31, 31	...		N91	
92	316.5+21.2	0.019	0.11 (0.01)	−5.60 (0.06)	1.52 (0.15)	ND[1] −6.1[2]	Ju92b	Y
93	316.5-4.0	0.030	0.13 (0.02)	−6.49 (0.04)	0.66 (0.10)		N91	
94	316.9-4.9	0.023	...	−101, 101	...		Ju92c	
95	316.9-2.1	0.047	...	−29, 33	...		N91	
96	317.0-4.6	0.016	0.07 (0.01)	−6.33 (0.05)	0.54 (0.11)		Ju92b	
97	319.9-4.8	0.020	...	−31, 31	...		A90	Y
98	320.1-4.3	0.031	...	−31, 31	...		N91	Y
99	320.5-3.5	0.029	...	−48, 52	...		M93a	Y
100	320.5-3.6	0.028	0.15 (0.02)	−0.61 (0.03)	0.61 (0.08)		N91	Y
101	320.7-1.7	0.029	0.11 (0.03)	−0.33 (0.08)	0.59 (0.19)		N91	Y
102	320.7-2.0	0.024	...	−101, 101	...		Ju92c	
103	320.9-2.1	0.054	...	−36, 26	...		N91	
104	322.7+4.0	0.035	...	−31, 31	...		M93b	
105	322.7+3.9	0.026	...	−101, 101	...		Ju92b	
106	323.0+4.0	0.029	...	−36, 26	...		N91	Y
107	325.2+5.8	0.039	0.15 (0.03)	−5.75 (0.05)	0.29 (0.11)		N91	Y
108	325.9+5.9	0.028	...	−101, 101	...		Ju92c	
109	326.8+5.6	0.027	...	−101, 101	...		Ju92c	Y
110	326.9+5.5	0.019	0.10 (0.01)	−10.41 (0.04)	0.52 (0.08)	ND[2]	Ju92c	Y
111	327.2+1.8	0.024	0.49 (0.01)	0.00 (0.01)	0.71 (0.02)		Ju92a	
112	330.7-1.3	0.023	...	−101, 101	...	−4.8[2]	Ju92c	Y
113	331.0-0.7	0.021	0.20 (0.01)	−5.07 (0.02)	0.77 (0.05)		Ju92c	
114	331.1-2.3	0.025	...	−101, 101	...		Ju92c	
115	332.7+6.8	0.022	...	−50, 50	...		Ju92a	Y
116	334.2+0.0	0.021	0.10 (0.01)	−20.28 (0.03)	0.81 (0.07)		Ju92c	
117	334.6+4.6	0.034	0.17 (0.02)	3.52 (0.04)	0.61 (0.09)	3.6[2]	N91	Y
118	334.6-1.4	0.026	...	−101, 101	...		Ju92c	Y
119	335.9+7.0	0.030	...	−50, 50	...	4.0[2]	M93a	
120	336.7+7.8	0.020	...	−101, 101	...		Ju92c	

Table 1. *Continued.*

Number	DC Name	rms (K)	T_a^* (K)	V_{lsr} [a] (km s^{-1})	ΔV (km s^{-1})	V_{other} [b] (km s^{-1})	Session[c]	*IRAS* [d]
121	337.1-4.9	0.029	...	−51, 11	...	ND[2]	N91	Y
122	337.7-4.0	0.033	0.16 (0.02)	3.59 (0.05)	0.65 (0.11)	3.5[2]	N91	
123	337.8-1.6	0.024	...	−101, 101	...	−10.7[2]	Ju92c	
124	337.9-1.4	0.023	...	−101, 101	...		Ju92c	
125	338.2+0.8	0.023	...	−101, 101	...		Ju92c	Y
126	338.6+9.5	0.032	...	−101, 101	...		Ju92c	Y
127	338.6+11.9	0.030	...	−50, 50	...		M93a	
128	339.1+11.7A	0.030	...	−101, 101	...		Ju92c	
129	339.1+11.7B	0.027	...	−101, 101	...		Ju92c	
130	339.1-0.8	0.029	0.11 (0.02)	−30.17 (0.04)	0.35 (0.09)		N91	
131	339.3-0.3	0.020	...	−101, 101	...		Ju92c	Y
132	340.4+5.5	0.025	0.13 (0.02)	4.61 (0.03)	0.39 (0.06)		Ju92c	
133	340.5+0.5	0.050	0.23 (0.04)	5.11 (0.04)	0.47 (0.10)	5.0[2] 4.9[4]	N91	
134	340.9+9.2	0.026	...	−101, 101	...		Ju92c	
135	343.4+3.5	0.027	0.08 (0.02)	4.53 (0.06)	0.64 (0.15)	4.72[4]	N91	
136	344.5+2.0	0.027	...	−31, 31	...		N91	Y
137	344.6-4.3	0.026	0.17 (0.01)	−12.51 (0.04)	1.40 (0.10)	ND[2]	Ju92c	Y
138	345.0-3.5	0.012	0.12 (0.01)	7.66 (0.04)	0.92 (0.10)		Ju92b	Y
139	345.2-3.6	0.037	...	−50, 50	...		Ju92a	Y
140	345.4-4.0	0.040	0.96 (0.02)	−8.32 (0.01)	1.42 (0.03)	−8.2[2]	Ju92b	Y
141	345.8+7.6	0.028	...	−101, 101	...		Ju92c	
142	346.2-11.7	0.052	0.19 (0.04)	−22.75 (0.06)	0.65 (0.13)		N91	
143	346.4-5.0	0.028	...	−101, 101	...		Ju92b	
144	346.4+7.9	0.020	0.07 (0.01)	3.73 (0.05)	0.64 (0.12)		Ju92c	
145	347.5-8.0	0.058	0.31 (0.04)	7.65 (0.03)	0.62 (0.08)	7.3[2]	N91	
146	347.9-4.4	0.040	...	−31, 31	...		N91	
147	348.0+3.7	0.020	...	−31, 31	...		A90	
148	349.0+3.0	0.033	...	−31, 31	...		Ja91b	Y
149	349.2+3.1A	0.032	0.09 (0.02)	10.86 (0.08)	0.98 (0.19)		N91	Y
150	349.2+3.1B	0.030	...	−31, 31	...		N91	Y
151	349.3+3.1	0.028	...	−101, 101	...		Ju92c	Y
152	351.0+3.9	0.029	...	−101, 101	...		Ju92c	
153	351.2+5.1	0.029	...	−35, 65	...		M93a	Y
154	351.2+5.2	0.032	0.11 (0.02)	17.19 (0.06)	0.56 (0.13)	ND[4] 18.52[6]	Ju92c	Y
155	351.7+0.5	0.029	...	−101, 101	...	5.8[4]	Ju92c	Y
156	351.8+2.8	0.055	...	−101, 101	...		Ju92c	Y
157	352.9+4.8	0.029	...	−101, 101	...	13.77[6]	Ju92c	Y
158	352.9+5.0	0.022	...	−101, 101	...		Ju92c	Y
159	353.1+2.3	0.018	0.08 (0.02)	7.91 (0.11)	1.26 (0.25)		Ja91a	Y
160	353.3+2.4	0.032	...	−101, 101	...		Ju92c	Y
161	353.5+3.5	0.028	...	−50, 50	...		M93a	Y
162	354.1+2.9A	0.040	...	−101, 101	...		Ju92c	
163	354.1+2.9B	0.031	0.11 (0.01)	12.05 (0.05)	0.73 (0.11)		Ju92a	
164	354.1+2.9C	0.023	0.06 (0.01)	11.39 (0.11)	1.31 (0.25)		Ju92a	Y
165	354.1+2.9D	0.017	0.05 (0.01)	9.77 (0.14)	1.30 (0.34)		Ju92b	
166	354.1+2.9E	0.020	0.05 (0.01)	11.85 (0.09)	1.29 (0.21)		Ju92c	
167	354.2+3.2	0.031	...	−101, 101	...		Ju92c	Y
168	356.5-4.5	0.028	...	−101, 101	...		Ju92c	Y
169	4.9-24.6	0.028	...	−61, 1	...		N91	
169		0.045	...	−1, 61	...		N91	
–	B68[e]	0.026	0.51 (0.05)	3.41 (0.01)	0.28 (0.01)	3.2[7] 3.31[8]	A90	

Notes.

[a] When no signal was detected the velocity range observed is given.

[b] [1]Zealey et al. (1983); [2]Goss et al. (1980); [3]de Vries et al. (1984); [4]Sandqvist & Lindroos (1976); [5]Kuiper et al. (1987); [6]Clemens et al. (1991); [7]Martin & Barrett (1978); [8]BM; ND indicates the cloud was not detected.

[c] A90: 1990 August/September ($\Delta v = 0.25$ km s^{-1}); Ja91a: 1991 January ($\Delta v = 0.25$ km s^{-1}); Ja91b: 1991 January ($\Delta v = 0.12$ km s^{-1}); N91: 1991 November ($\Delta v = 0.12$ km s^{-1}); Ju92a: 1992 June ($\Delta v = 0.10$ km s^{-1}, 1024 channels); Ju92b: 1992 June ($\Delta v = 0.20$ km s^{-1}); Ju92c: 1992 June ($\Delta v = 0.10$ km s^{-1}, 2048 channels); M93a: 1993 March ($\Delta v = 0.20$ km s^{-1}); M93b: 1993 March ($\Delta v = 0.12$ km s^{-1}); F94: 1994 February ($\Delta v = 0.05$ km s^{-1}).

[d] Y indicates an associated *IRAS* source (Paper I).

[e] RA (1950.0) = 17^{h}19^{m}36^s, Dec. (1950.0) = −23°46′57″.

Martin & Barrett (1978), and 8 to BM. Column 8 indicates the observing session when the spectrum was obtained and the velocity resolution (see table footnotes). Column 9 indicates whether there is an *IRAS* point source associated with the cloud as given by BHR.

The detection statistics are discussed in Section 5, in particular Section 5.1 where a comparison with the cores within complexes is presented.

Table 2 shows the results for the observations of the (2,2) transition for the strongest (1,1) sources ($T_a^* \geq 0.35$ K) in Table 1. In this table, column 1 lists the cloud number and column 2 the cloud name. Column 3 lists the rms noise level in the off-channels as in Table 1. Columns 4–6 give the results of the Gaussian fits to the (2,2) line when it was visible, with the uncertainties quoted in parentheses. In the two cases where the (2,2) line was not detected the velocity of the central channel is given.

The sources in Table 2 were mapped on a 1-arcmin grid; the results of this mapping are given in Table 3. In this table, column 1 lists the cloud number and column 2 the cloud name. Columns 3 and 4 list the major and minor axes of the half-power contour of the ammonia map; it has been found that all the mapped globules may in fact be reasonly approximated by an ellipse. Column 5 gives the aspect ratio (major axis/minor axis) and column 6 the beam filling factor as determined by equation (3) below. Columns 7 and 8 then give the cloud size in arcminutes and parsecs respectively, where the cloud size is the geometric mean half-power diameter as derived from the major and minor axes. The cloud sizes presented here have been corrected for the telescope beamsize by assuming that the observed cloud size is the quadrature sum of the true cloud size and the telescope beam, with the map and beamshapes assumed to be Gaussian. Column 9 quotes the adopted distance to the cloud used to determine its linear size (see Section 3.2 below). A full analysis and interpretation of the mapping results will be presented in Paper III.

Table 2. Results of (2,2) observations for the strongest (1,1) sources from Table 1.

Number	DC Name	rms (K)	T_a^* (2,2) (K)	V_{lsr} (km s^{-1})	ΔV (km s^{-1})
8	253.1–1.7A	0.022	0.11 (0.02)	6.07 (0.04)	0.50 (0.09)
12	253.3–1.6	0.037	0.17 (0.02)	6.21 (0.06)	0.81 (0.13)
36	267.4–7.5	0.032	0.19 (0.03)	5.18 (0.04)	0.58 (0.09)
41	267.7–7.4	0.023	0.10 (0.01)	5.29 (0.04)	0.49 (0.11)
55	275.9+1.9	0.024	...	–4.00	...
68	295.0+3.4	0.021	0.07 (0.01)	–8.07 (0.05)	0.36 (0.13)
71	297.7–2.8	0.028	0.22 (0.01)	–4.40 (0.04)	0.66 (0.10)
86	303.8–14.2	0.070	0.37 (0.09)	3.03 (0.05)	0.35 (0.13)
111	327.2+1.8	0.024	...	2.00	...
140	345.4–4.0	0.025	0.16 (0.03)	–8.65 (0.11)	0.75 (0.18)
–	B68	0.020	0.10 (0.02)	3.35 (0.08)	0.70 (0.19)

Table 3. Mapping results.

Number	DC Name	Major Axis (′)	Minor Axis (′)	Aspect Ratio	ϕ	d (′)	d (pc)	$D^{(a)}$ (pc)
8	253.1–1.7A	3.5	1.8	1.9	0.73	2.5	0.29	400[1]
12	253.3–1.6	2.3	1.6	1.4	0.64	1.9	0.22	400[1]
36	267.4–7.5	4.2	2.4	1.8	0.82	3.2	0.37	400[1]
41	267.7–7.4	2.1	1.9	1.1	0.67	2.0	0.23	400[1]
55	275.9+1.9	3.2	2.3	1.4	0.78	2.7	0.24	300[2]
68	295.0+3.4	3.3	1.9	1.7	0.74	2.5	0.26	350[2]
71	297.7–2.8	3.5	2.1	1.7	0.77	2.7	0.14	175[3]
86	303.8–14.2	2.4	1.4	1.7	0.61	1.8	0.11	200[4]
111	327.2+1.8	2.3	1.4	1.6	0.60	1.8	0.13	250[2]
140	345.4–4.0	1.9	1.9	1.0	0.65	1.9	0.22	400[2]
–	B68	2.1	1.4	1.5	0.59	1.7	0.10	200[5]

Notes: [a][1]Vela CG; [2]from stellar reddening; [3]proximity to Coalsack; [4]proximity to Chamaeleon II (Hughes & Hartigan 1992); [5]Bok (1977).

3 DATA ANALYSIS

3.1 Ammonia analysis: model fitting and derivation of properties

Where the satellite features were clearly visible in the spectra, they were fitted with the 18 hyperfine components of the (1,1) transition (see e.g. Ungerechts, Walmsley & Winnewisser 1980). This allows for the determination of the line optical depth, $\tau(1,1,m)$, where the letter m denotes the main hyperfine group, the line velocity, V_{lsr}, and the intrinsic FWHM linewidth ΔV. This model fitting should not be confused with the single-component Gaussian fits given in Table 1. The fitting program, NH$_3$FIT, in SPC is a least-squares fit based on the fitting routine CURFIT of Bevington (1969). It is similar to that used by other authors (see e.g. Pauls et al. 1983; BM), and is therefore not discussed here. An example of a spectrum where the satellites are clearly visible (DC 327.2 + 1.8 = BHR 111) and its best-fitting model spectrum are shown in Fig. 1.

In analysing the ammonia data, there are a number of steps which have been followed: the derivation of excitation temperatures, column densities, rotation and kinetic temperatures; and the derivation of molecular hydrogen densities and cloud masses. The determination of excitation temperature, column densities and kinetic temperature outlined below follows closely that of Harju, Walmsley & Wouterloot (1993).

3.1.1 *Excitation temperature*

If the optical depth $\tau(1,1,m)$ is known then the excitation temperature T_{ex} of the (1,1) transition may be derived from the relation

$$T_a^* = \eta\phi \frac{h\nu}{k} [F(T_{ex}) - F(T_{bg})][1 - e^{-\tau(1,1,m)}], \quad (1)$$

where T_a^* is the corrected antenna temperature, η the beam efficiency, ϕ the beam filling factor and T_{bg} the cosmic background temperature, taken to be equal to 2.7 K. The function $F(T)$ is defined to be

$$F(T) = \frac{1}{e^{h\nu/kT} - 1}. \quad (2)$$

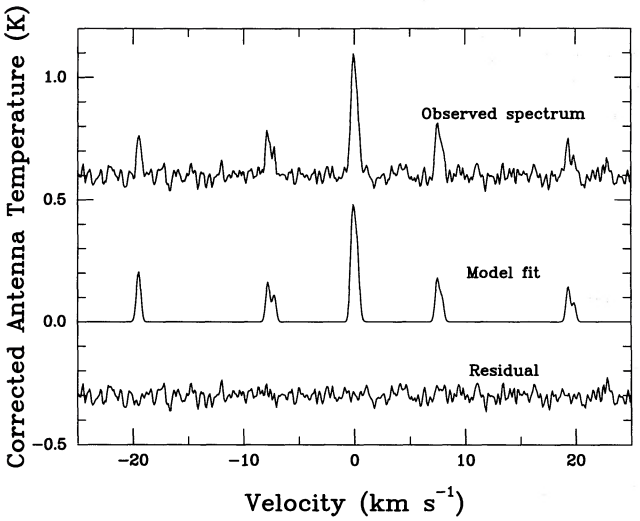

Figure 1. The observed NH_3 (1,1) spectrum of DC 327.2+1.8 (upper), the model best-fitting spectrum (centre) and the residual of the fit (lower), where the model has been subtracted from the spectrum. The observed spectrum is offset from the model spectrum by 0.6, and the residual is offset by −0.3. The splitting of the hyperfine components is clearly visible in this figure.

For the (1,1) transition $h\nu/k$ is equal to 1.14 K. For the mapped sources we were able to derive a core size, $\theta_x \times \theta_y$, where θ_x and θ_y are the major and minor axes respectively, in arcmin, of the map half-power contour. This assumes that the source shape may be well-approximated by an ellipse, which for almost all the sources presented here is certainly the case. The half-power contour thus defines the core. The beam filling factor ϕ may then be found from the relation (Benson 1983)

$$\phi = \left\{\left[1+\left(\frac{\theta_b}{\theta_x}\right)^2\right]\left[1+\left(\frac{\theta_b}{\theta_y}\right)^2\right]\right\}^{-1/2}, \tag{3}$$

where θ_b is the FWHM of the telescope beam. For sources that we have not mapped and for which we have therefore not been able to deduce a filling factor, an average value of ϕ based on the mapped sources in this work (see Table 3) has been assumed.

3.1.2 *Column densities*

To obtain the column density of molecules in the upper (1,1) state we assume that all the hyperfine components have the same excitation temperature, and that the excitation conditions along the line of sight are uniform. The column density in the upper state is then given by

$$N_u(1,1) = 1.6\times10^{13} F(T_{ex})\,\Delta V \tau(1,1,m), \tag{4}$$

where ΔV is in km s^{-1}. For some sources it is not possible to determine N_u using equation (4), as a result of a low signal-to-noise ratio not allowing an opacity estimate, or because the model fit implies a small optical depth. In these cases, if it is assumed that optically thin conditions prevail, N_u may be estimated by integrating over the (1,1) satellites, or in cases where they are not visible, by integrating over the main group. In practice one has to calculate the area under the observed line or lines, which is aided greatly by first applying the fitting program to identify the satellite lines. In this case the column density is given by

$$N_u(1,1) = \frac{1}{\phi}\,1.3\times10^{13}\,\frac{1}{1-\dfrac{F(T_{bg})}{F(T_{ex})}}\int T_B(1,1,s)\,\mathrm{d}V, \tag{5}$$

where $T_B = T_a^*/\eta$ is the beam brightness temperature, and the letter s refers to the satellite lines. The integral is over all four satellite groups. Equation (5) still applies when integrating over the main-line group instead of the satellites. For the (2,2) line the integral is over the main line only and the numerical factor in equation (5) is 6.1×10^{12}.

The total number of molecules in the (1,1) state is then found by assuming a Boltzmann distribution between the upper and lower states, and so the (1,1) column density is given by

$$N(1,1) = N_u + N_l = N_u(1+\mathrm{e}^{h\nu/kT_{ex}}), \tag{6}$$

where N_l is the column density in the lower state.

3.1.3 *Rotation and kinetic temperatures*

If the (2,2) transition has been observed then it is possible to determine the rotation temperature T_R between the (1,1) and (2,2) transitions from

$$\frac{N(2,2)}{N(1,1)} = \frac{5}{3}\,\mathrm{e}^{-\Delta E/kT_R}, \tag{7}$$

where the factor of 5/3 is the ratio of statistical weights and $\Delta E/k = 41.5$ K is the temperature corresponding to the energy difference between the (1,1) and (2,2) states. The rotation temperature may also be calculated directly from the observed antenna temperatures and the optical depth of the (1,1) line, $\tau(1,1,m)$, when it has been derived (Ho & Townes 1983):

$$T_R = \frac{-\Delta E/k}{\ln\left\{\dfrac{-0.282}{\tau(1,1,m)}\ln\left[1-\dfrac{T^*(2,2,m)}{T_a^*(1,1,m)}\left(1-\mathrm{e}^{-\tau(1,1,m)}\right)\right]\right\}}. \tag{8}$$

In principle the values of T_R calculated from equations (7) and (8) should be identical. In practice we find that they agree within the limits of their uncertainties. Values found from equation (7) have been used in this work, except when the (2,2) line was not detected, in which case equation (8) has been used with 3σ upper limits to $T_a^*(2,2)$.

The rotation temperature slightly underestimates the kinetic temperature in the cold dark clouds, and the deviation between the two becomes greater at higher temperatures. The kinetic temperature, T_K, may be found from the three-level equation of Walmsley & Ungerechts (1983), using the rate constants calculated by Danby et al. (1988) for the rotational excitation of NH_3 by H_2,

$$T_R = \frac{T_K}{1+\dfrac{kT_K}{\Delta E}\ln\left(1+\dfrac{C_{23}}{C_{21}}\right)}, \tag{9}$$

where C_{23} represents the rate of collisional transfer of population between the (2,2) and (2,1) levels and C_{21} the rate

between the (1,1) and (2,2) levels. The (2,1) population is considered to be negligible compared with that of the (1,1) level.

The total column density of ammonia molecules is found by assuming that the metastable ($J=K$) levels are the only ones populated. The expression for the total column density $N(NH_3)$ is then

$$N(NH_3)=N(1,1)\left(\frac{1}{3}e^{23.4/T_R}+1+\frac{5}{3}e^{-41.5/T_R}+\frac{14}{3}e^{-101.5/T_R}\right), \quad (10)$$

where the terms greater than the (3,3) level have been ignored, as they are insignificant at the temperatures of a typical dark cloud core (~ 10 K).

3.1.4 *Densities, abundances and masses*

With T_{ex} and T_K known, the local molecular hydrogen number density may then be found by balancing collisions and stimulated and spontaneous emission (Ho & Townes 1983):

$$n(H_2)=\frac{A}{C}\frac{F(T_{ex})-F(T_{bg})}{F(T_K)-F(T_{ex})}[1+F(T_K)], \quad (11)$$

where A is the Einstein A coefficient, which is 1.7×10^{-7} s^{-1} for the (1,1) transition, and C is the collisional de-excitation rate of the (1,1) transition, which is equal to 8.5×10^{-11} cm^3 s^{-1} at the temperatures derived here (Danby et al. 1988). We are then able to determine the fractional abundance of ammonia, $\chi(NH_3)$, which for a homogeneous cloud is given by

$$\chi(NH_3)\sim\frac{N(NH_3)}{2dn(H_2)}, \quad (12)$$

where d is the cloud diameter, taken by Harju et al. (1993) to be the half-power diameter at the peak intensity.

There are two ways to determine the core masses. The first makes use of the local molecular hydrogen density and assumes that the cores are homogeneous and spherical clumps with radii estimated from the map half-power contour. The mass is then found from

$$M(r)=\frac{4\pi}{3}r^3n(H_2)\langle m\rangle, \quad (13)$$

where r is the cloud radius and $\langle m\rangle=4.3\times10^{-24}$ g (Genzel 1991) is the mean mass per hydrogen molecule, including heavier elements. Assuming that the ammonia column density and abundance are known, the core mass may also be estimated from the hydrogen column density $N(H_2)$, using the relation

$$M(r)=\frac{2\pi}{3}r^2N(H_2)\langle m\rangle. \quad (14)$$

If the core size is not known, the above equation can be used to estimate the beam-averaged mass (i.e. the mass within the telescope beam) from the beam-averaged column density, $\langle N(H_2)\rangle=\phi[N(H_2)]$, and the beamsize.

3.2 Distances

In order to determine the physical sizes and masses of the clouds, their distances have to be determined. For this work a number of methods have been used to estimate the cloud distances. For example, clouds that appear to be visually associated with the Coalsack, and that have similar ammonia velocities ($V_{lsr}\sim-5$ km s^{-1}), are assumed to lie at a similar distance of 175 pc (Rodgers 1960). The Vela cometary globules are assumed to lie at a common distance of 400 pc (Herbst 1977).

For clouds whose distances cannot be estimated on the above basis, the distribution of stellar reddening in the direction of the dark cloud is utilized. The central idea behind this method is that the dark clouds exist in large groups and are located in discrete layers with respect to distance from the Sun (see e.g. Lynds 1968; Dickman & Clemens 1983), and that these layers may be traced over many square degrees on the sky. A plot of the stellar reddening of a sufficiently large number of stars in a given region against their distance corrected for reddening will thus show 'steps' of reddening at one or more discrete distances, implying the existence of an intervening cloud or group of clouds at each step. The colours and spectral types of a large number of stars are thus needed for this method to work successfully.

The stellar reddening, $E(B-V)$, may be determined if $(B-V)$ is known, and if the MK spectral type and hence the star's intrinsic colour, $(B-V)_0$, are also known. The distance modulus corrected for the reddening may then be found by assuming some value for the ratio of total-to-selective extinction, $A_V/E(B-V)$, where A_V is the visual extinction. In this paper this ratio is taken to be equal to 3.1 (Rieke & Lebofsky 1985).

Large areas of sky must be searched to obtain enough stars for plotting, because of the limited number of stars for which MK spectral types and colours are available. Snell (1981) used a region of $20°\times20°$ centred on his cloud positions, and Dickman & Clemens (1983) searched a region of $11°\times16°$ in their study. In this study, the MK Classification Extension Catalogue of Morris-Kennedy (1983) has been examined for stars lying within a given radius centred on the globule. Since this catalogue is available in electronic form, the procedure has been greatly simplified, and allows for a quick search of a small area around the globule in the hope of finding a sufficient number of stars. Larger areas may then be used if an insufficient number of stars have been found. Where possible a search radius of 5° has been used. If not enough stars are found, the radius is increased to 7°.5, and then to 10° if necessary. It is also possible to use common search areas for spatially associated globules with similar velocities, with the assumption that they lie at a similar distance. As an example of the technique, a plot of reddening against distance is shown in Fig. 2 in the direction of the dark cloud DC 345.4−4.0 (BHR 140), for which a distance of ~400 pc has been determined.

One shortcoming of the above method is the uncertainty in deciding to which cloud layer the small globules belong, particularly considering the large search areas used. In some instances more than one step in reddening may occur, indicating more than one layer of intervening matter. Without any knowledge to the contrary, it is assumed that the dense globules are associated with the nearest obscuration,

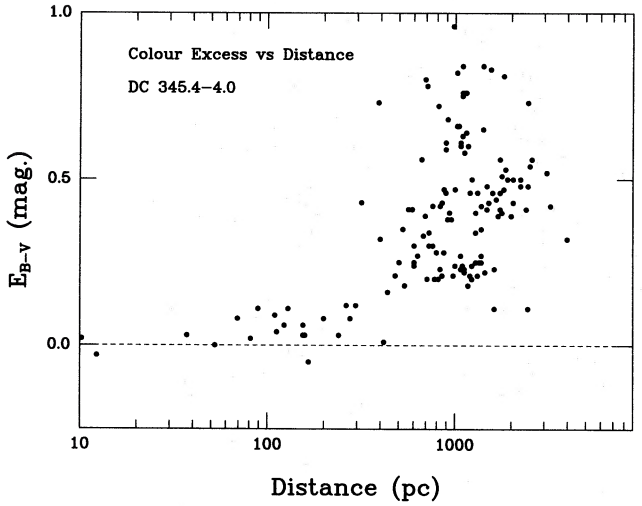

Figure 2. A plot of reddening against distance in the direction of the dark cloud DC 345.4 − 4.0. A discontinuity in the reddening is evident at a distance of about 400 pc, indicating the probable cloud distance.

since their opaqueness and the general lack of foreground stars imply that they are among the closest clouds in that direction. Distances derived for a number of globules are given in Tables 4 and 9 (see below).

4 DERIVED PROPERTIES OF THE CLOUDS

In Table 4 we present the fitted parameters and derived properties of those clouds whose ammonia spectra could be successfully modelled. In this table, column 1 lists the cloud number and column 2 the cloud name. Columns 3 and 4 give the velocity with respect to the local standard of rest (V_{lsr}) and the intrinsic FWHM ammonia linewidth (ΔV), derived from the 18-component model fit (which, it should be noted, are not the same as the values determined from the single-component Gaussian fit of the main-line group given in Table 1). Column 5 indicates the value of the optical depth derived from the best-fitting spectrum, and column 6 the derived excitation temperature. Column 7 lists the column density of the (1,1) transition. Column 8 lists the value of T_R used, and column 9 the total column density of NH_3. Column 10 lists the derived values of T_K and column 11 lists the derived values of $n(H_2)$. Column 12 lists the beam-averaged column density, and column 13 the assumed cloud distance, which is found from stellar reddening as described in Section 3.2, unless otherwise indicated. Column 14 lists the core mass, where the core radius is either found from mapping the source or, for the cometary globules that have not been mapped, assumed to be equal to the optical size. Column 15 indicates the beam-averaged mass.

We were able to fit successfully the ammonia hyperfine spectra for only 14 of the sources listed in Table 1 (including B68). For these we were able to derive both the opacity and the excitation temperature. Another 20 sources have hyperfine components visible in their spectra, but the model fit implies either a very small optical depth or a low signal-to-noise ratio, or that the uncertainties in the fit are large [> 30 per cent, usually a result of the hyperfine components having varying heights, perhaps implying non-LTE conditions (see e.g. Stutzki et al. 1984; Stutzki & Winnewisser 1985)]. For these sources the integral over the hyperfine components has been used to determine the column densities. For spectra where equation (4) was applied, the results have been compared with those derived from equation (5). The results in almost all cases are similar, as a result of the optical depths usually being small. In cases where the excitation temperature cannot be derived, however, a value must be assumed in order to calculate N_u. Harju et al. (1993) used an average value of T_{ex} from positions where they were able to determine it. For our sources the average value of T_{ex} is ~6 K, while for the BM sources the average is ~7 K. In the analysis presented here, T_{ex} is taken to be 6 K when it has not been determined directly, and so the term $f(T_{ex}) \equiv [1 - F(T_{bg})/F(T_{ex})]^{-1}$ in equation (5) is equal to 1.7. For the weaker sources, where an attempt has been made to fit the spectra (with varying degrees of success), the derived excitation temperatures are usually lower than those determined for the stronger sources (the optical depths are usually similar), and so to set $T_{ex} = 6$ K in order to place a lower limit on N_u appears to be a valid assumption for these sources. If one puts $T_{ex} = 10$ K then $f(T_{ex}) = 1.3$ (as used by Harju et al. 1993), which results in a lower, but not significantly different, result from that found with $T_{ex} = 6$ K. The uncertainties in the calibration of the spectra (estimated by many authors to be of the order of 20 per cent: e.g. Bachiller, Guilloteau & Kahane 1987) and in calculating the line areas that follow as a result imply that the choice of T_{ex} is not crucial, as long as it is kept significantly higher than T_{bg}, so that $f(T_{ex})$ is not significantly greater than unity.

For the 11 globules that have been mapped, the mean value for the filling factor is ~0.7 and this value has been assumed in the analysis as the beam filling factor for the unmapped sources. For comparison, BM found an average value of 0.7 for the sources that they mapped with the Haystack telescope, for which $\theta_b = 1.45$ arcmin.

In order to estimate the total column density of NH_3, we have assumed that $T_R = 10$ K when we have not been able to derive it, this value being based on our derived values of T_R for other globules and those determined in previous studies. For the cometary globules when we were not able to derive T_R directly, we have assumed a value of 13 K, based on the derived values for the other cometary globules. The column densities are not highly sensitive to the value of T_R used. In determining the core masses, half of the half-power cloud diameter has been used as the cloud radius.

The determination of the total density requires a knowledge of both the kinetic and excitation temperatures. In some cases it has been possible to determine only one of these temperatures, and so in order to estimate the density the other temperature has been assumed. These cases are indicated in Table 4.

For clouds where the core sizes are unknown, we have determined the beam-averaged mass (i.e. the mass within the telescope beam) from the beam-averaged column density and equation (14), assuming an ammonia abundance of 3×10^{-8}, which is the average value derived for the clouds in this work, where we have been able to determine it. By comparison with masses derived from the core sizes, it can be seen that the beam-averaged mass is in most cases lower than the core mass. In cases where the cloud size is greater than the beamsize, for example the cores that we have

Table 4. Derived parameters from ammonia spectra.

Number	DC Name	V_{lsr} (km s^{-1})	ΔV (km s^{-1})	$\tau(1,1,m)$	T_{ex} (K)	$N(1,1)^{(a)}$ ($\times 10^{13}$ cm^{-2})	$T_R{}^{(b)}$ (K)	$N(NH_3)$ ($\times 10^{14}$ cm^{-2})	$T_K{}^{(c)}$ (K)	$n(H_2)^{(d)}$ ($\times 10^3$ cm^{-3})	$<N(H_2)>^{(e)}$ ($\times 10^{21}$ cm^{-2})	$D^{(f)}$ (pc)	$M^{(g)}$ ($M_\odot$)	$<M>$ ($M_\odot$)
12	253.3–1.6	6.18	0.80	1.0	7.6	17.6†	13	5.4	14	20.0	11.5	400[1]	7.1	3.3
36	267.4–7.5	5.29	0.73	0.9	5.2	9.9†	16	2.6	18	6.4	7.1	400[1]	11	2.0
41	267.7–7.4	5.37	0.44	2.4	6.6	19.8†	9.4	10.0	9.6	23.1	22.3	400[1]	9.3	6.4
55	275.9+1.9	–5.41	0.56	1.0	5.3	8.5†	12	2.9	13*	8.1	7.5	300	3.7	1.2
68	295.0+3.4	–7.55	0.57	1.2	5.0	9.7†	11	3.7	11	7.7	9.1	350	4.5	2.0
71	297.7–2.8	–4.45	0.74	1.7	7.9	27.0†	12	9.2	13	24.2	23.6	175[2]	2.2	1.3
86	303.8–14.2	3.67	0.47	1.4	8.8	16.3†	13	5.0	14	29.9	10.1	200[3]	1.3	0.7
111	327.2+1.8	0.00	0.41	1.3	6.3	9.3†	11	3.6	11*	14.8	7.2	250	1.1	0.8
140	345.4–4.0	–8.35	1.02	2.4	7.9	53.1†	11	20.4	11	32.4	44.2	400	11	13
–	B68	3.41	0.28	2.0	5.9	9.2†	15	2.5	16	9.1	4.9	200[4]	0.3	0.4
5	252.2+0.7					6.5	(13)	2.0			4.7	400[1]		1.3
7	252.5+0.1	4.84	0.61	1.8	3.9	12.0†	(13)	3.7	(14)	3.0‡	8.6	400[1]	1.4	2.5
8	253.1–1.7A					7.6	14	2.2	14	10.3‡	5.4	400[1]	8.3	1.5
9	253.1–1.7B					3.2	(13)	1.0			2.3	400[1]		0.7
13	253.6+2.9					4.3	(13)	1.3			3.0	400[1]		0.9
14	253.8–10.9	–1.05	0.45	1.9	4.0	9.6†	(13)	3.0	(14)	3.3‡	7.0	400[1]	0.9	2.0
17	256.2–14.1					3.4	(13)	1.1			2.6	400[1]		0.7
23	259.9–0.0					10.4	(10)	4.7			11.0	500		4.9
25	260.7–12.4					5.6	(13)	1.7			4.0	400[1]		1.1
28	262.9–15.5	–0.69	0.52	1.9	3.9	10.6†	(13)	3.3	(14)	3.0‡	7.7	400[1]	0.5	2.2
34	267.2-7.2					3.5	(10)	1.6			3.7	400[1]		1.1
37	267.5–7.4	6.05	0.60	1.4	4.5	10.7†	(13)	3.3	(14)	4.8‡	7.7	400[1]	2.0	2.2
38	267.6–6.0A					4.0	(10)	1.8			4.2	450		1.5
53	274.2–0.4					4.0	(10)	1.8			4.2	500		1.9
58	289.3–2.8					5.3	(10)	2.4			5.6	250		0.6
59	291.1–1.7					3.7	(10)	1.7			4.0	250		0.4
64	293.3–0.9					9.1	(10)	4.1			9.6	900		14
74	300.0–3.7					2.9	(10)	1.3			3.0	175[2]		0.2
83	302.1+7.4					4.0	(10)	1.8			4.2	300		0.7
113	331.0–0.7					4.5	(13)	1.4			3.3	200		0.2
117	334.6+4.6					3.2	(10)	1.4			3.3	250		0.4
137	344.6–4.3					9.5	(10)	4.3			10.0	700		8.7
138	345.0–3.5					3.1	(10)	1.4			3.3	400		0.9
145	347.5–8.0					7.0	(10)	3.1			7.2	450		2.6

Notes.
[a]† indicates that $N(1,1)$ is determined from fit of model spectrum, otherwise $N(1,1)$ is determined from the integral over the satellite lines.
[b]If T_R is undetermined then a value of $T_R = 10$ K is assumed for globules, and 13 K is assumed for CGs (indicated by parentheses).
[c]* indicates 3σ upper limits to $T_a^*(2,2)$ used to determine T_K from equation (8).
[d]‡ indicates that $n(H_2)$ is determined assuming a value for one or other of T_{ex} or T_K.
[e]Beam-averaged column density.
[f]Distance estimates: [1]Vela CG; [2]proximity to Coalsack; [3]proximity to Chamaeleon II; [4]Bok (1977); others from reddening.
[g]Radius either found from mapping, or, for CGs, assumed to be equal to the cloud head radius when not mapped.

mapped and that are shown in Table 3, the beam-averaged mass represents a lower limit to the core mass.

5 DISCUSSION

5.1 Comparison with cores in complexes

We wish to investigate whether there are any important differences between cores found in dark cloud complexes and those found in small isolated dark clouds. The major study of dense cores in complexes was undertaken by Myers and co-workers during the 1980s, culminating in the publication of a major survey of dense cores for ammonia emission (BM). The following is a comparison between the results of BM and the survey undertaken here.

BM divided their survey results into four categories. They defined strong detections as those having $T_a^* \geq 0.35$ K, moderate detections as those with $0.35 > T_a^* > 3\sigma$, questionable detections as those with a possible signal in the range 2σ–3σ at the correct velocity, and the fourth group as those with no detectable emission. Because the efficiencies of the telescopes used in the BM survey and the current survey are similar (for Haystack, $\eta = 0.25$ at the time of the BM survey; for Parkes, $\eta = 0.32$), a comparison of the two samples based on T_a^* is valid. Any correction for the difference between the two efficiencies would lower the observed temperatures of our sources relative to those of BM. This would enhance the differences between the two samples noted below. In this work, 10 sources were found to be strong (6 per cent), 66 were found to be moderate (39 per cent), 8 had questionable detections (5 per cent) and 85 of the 169 clouds had no observable signal (50 per cent). These results, along with those of BM, are shown in Table 5. In this table, column 1 lists the type of detection, as indicated above, and columns 2, 3, 4 and 5 list respectively the number of each type of detection in this work, in the BM sample, in the BM sample with their Taurus sources removed, and in the BM sample with both their Taurus and Ophiuchus sources removed. The latter two subdivisions are introduced because, as explained below, the Taurus and Ophiuchus sources in the BM sample may introduce some bias into the detection statistics of cores in complexes.

Table 5. Results of survey for ammonia emission in southern dark clouds. Also shown are the results of Benson & Myers (1989).

Detection Type	This Work	BM	BM[a]	BM[b]
strong ($T_a^* \geq 0.35$ K)	10 (6%)	42 (28%)	29 (25%)	19 (23%)
moderate ($3\sigma < T_a^* < 0.35$ K)	66 (39%)	24 (16%)	21 (18%)	11 (13%)
weak ($T_a^* \sim 2$–3σ)	8 (5%)	12 (8%)	10 (9%)	10 (12%)
No Detection	85 (50%)	71 (48%)	54 (47%)	44 (52%)
Totals	169	149	114	84

Notes. [a]Taurus sources removed from sample. [b]Taurus and Ophiuchus sources removed from sample.

Several points are worth noting. First, the number of detections in both samples is similar at about 50 per cent. Some sources may not have been detected because they are too distant or too small compared with the beamsize, resulting in beam dilution, or because we have yet to observe the densest part of the cloud (for the larger clouds).

The number of strong sources is significantly less than that found by BM for the cores in complexes, with only 6 per cent of the globules in this survey being strong, while 28 per cent of the BM sample are strong detections. BM include in their sample many cores from the Taurus and Ophiuchus dark clouds, which are nearby (~ 150 pc) and are known to be undergoing relatively efficient star formation. It may be that the cores in these clouds are significantly affecting the BM statistics, since it is unlikely that many of the globules lie this close to the Sun. To test this, Table 5 also shows the BM results with the Taurus and Ophiuchus sources removed. It can clearly be seen that the removal of these sources has not significantly changed the detection statistics of BM. The comparison therefore indicates that cores in complexes generally appear brighter in ammonia emission than cores found in isolated globules. The most obvious reason would seem to be that cores found within complexes are denser, as a result of their interactions with the dark cloud in which they are located.

Table 6 shows a comparison of a number of properties determined for the globules surveyed here and the cores within complexes. In cases where BM have analysed more than one point within a core, we have quoted the position of peak antenna temperature in this table to be consistent with the derivations listed in Table 4. Column 1 lists the property under consideration, column 2 the mean value for the globules, and column 3 the mean for the BM cores. The uncertainties quoted in this table are the standard errors in the mean.

Table 6. Comparison between various parameters for the cores within globules and those within complexes. The values in parentheses indicate the number of sources used in determining the mean values.

Property	Globules	BM Cores
τ_o	3.2 ± 0.3 (14)	6.2 ± 0.5 (38)
T_{ex} (K)	5.9 ± 0.4 (14)	7.1 ± 0.3 (38)
T_K (K)	12.9 ± 0.7 (11)	10.8 ± 0.4 (27)
$\log N^{(a)}$	14.4 ± 0.1 (34)	14.8 ± 0.1 (38)
$\log n^{(b)}$	4.1 ± 0.1 (15)	4.5 ± 0.1 (38)
d (pc)[c]	0.21 ± 0.02 (11)	0.21 ± 0.03 (33)
M ($M_\odot$)	4 ± 1 (15).	10 ± 2 (32)[d]

Notes.
[a] $N(NH_3)$ expressed in cm^{-2}.
[b] $n = 1.2n(H_2)$ expressed in cm^{-3}.
[c] Half-power contour of the ammonia contour map defines the core size.
[d] L1031B excluded from calculation ($M = 167 M_\odot$).

One way to test the idea that the cores within complexes are denser is to examine the opacities and excitation temperatures of the two samples. Equation (1) shows the relationship between the measured intensity from the cloud (the antenna temperature), the excitation temperature of the transition and the opacity. Equation (11) then shows how the density of the cloud affects the excitation temperature. For the globules we find that the average value of the derived total optical depth of the (1,1) transition, $\tau_o[=2\tau(1,1,m)]$, is 3.2 ± 0.3, while for the BM sample $\tau_o = 6.2 \pm 0.5$. (The histograms of the two samples are shown in Fig. 3). The cores in complexes thus show a greater opacity in the (1,1) line of ammonia. This should come as no surprise, since we know that the cores in complexes are surrounded by a medium which is denser than the general interstellar medium surrounding the isolated globules. If we assume that the ammonia abundance along the line of sight in the clouds is constant (see e.g. Turner 1993) then the inter-core medium in complexes can contribute to the observed optical depth. The difference in mean optical depth could also be a result of differences in excitation temperature (as noted above), linewidth, or column density between the two types of cores [see equation (4)].

The average value of the excitation temperature for the globules in this work is ~6 K, which is probably an upper limit for the weaker sources, as has been discussed in Section 4. For the BM sample $T_{ex} \sim 7$ K, and so the excitation temperature of the cores in complexes is also on average greater than that found in globules. Equation (1) thus shows that we should expect the measured intensity to be lower on average for the globules. It should then follow that the density derived for the globules is also lower, since it depends more strongly on the excitation temperature than on the kinetic temperature [equation (11)]. Table 6 shows that the kinetic temperature of the globules is larger than that of the BM cores, mainly as a result of the large values of T_K for the cometary globules skewing the mean globule value to a value slightly greater than the mean for the cores. That the density of the globules is lower is suggested by the ammonia column densities of the two samples, as shown in Table 6 and Fig. 4. For the globules the average is $\log N = 14.4 \pm 0.1$ (34 sources), while, for BM, $\log N = 14.8 \pm 0.1$ (38 sources). More conclusive is the fact that 82 per cent of the globules have $\log N \leq 14.6$ while 74 per cent of the cores in complexes have $\log N > 14.6$.

For the sources where we have been able to determine the total density we find an average value of $\log n = 4.1 \pm 0.1$ (15 sources), where $n = 1.2n(H_2)$. For the cores in complexes we find $\log n = 4.5 \pm 0.1$ (38 sources). The densities of the cores within complexes are thus on average more than twice that found in the isolated globules. It can be seen in Fig. 5 that the globules occupy a distinctly different region from the cores. In the analysis above, in order to facilitate a direct comparison between the two samples, the densities of the BM sources have been determined by using equation (11) and the values of T_{ex} and T_K quoted by BM, rather than by using the densities derived by BM from their large velocity gradient model. Application of the Kolmogorov–Smirnov two-sample test to the density data indicates that the probability that the globules and cores within complexes are subsamples of the

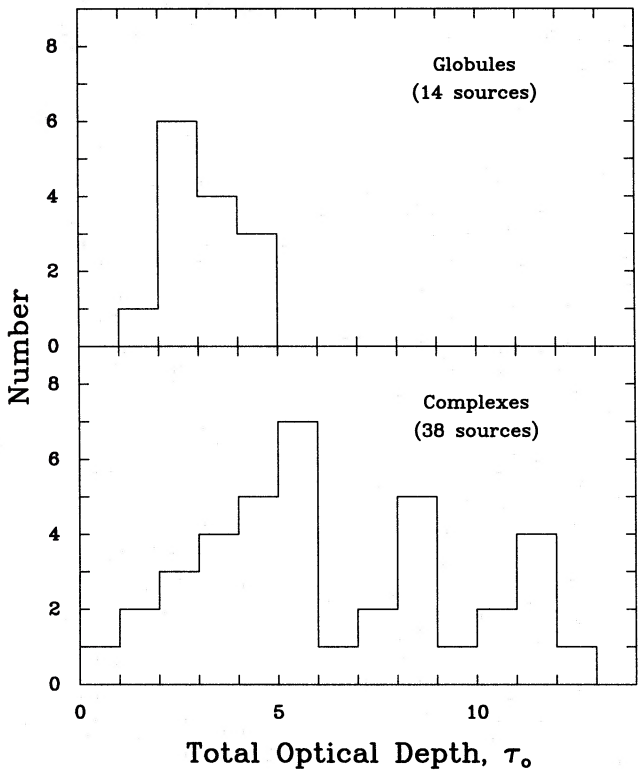

Figure 3. Histograms of the total optical depth of the (1,1) inversion transition of NH_3 for globules (upper) and cores within complexes (lower).

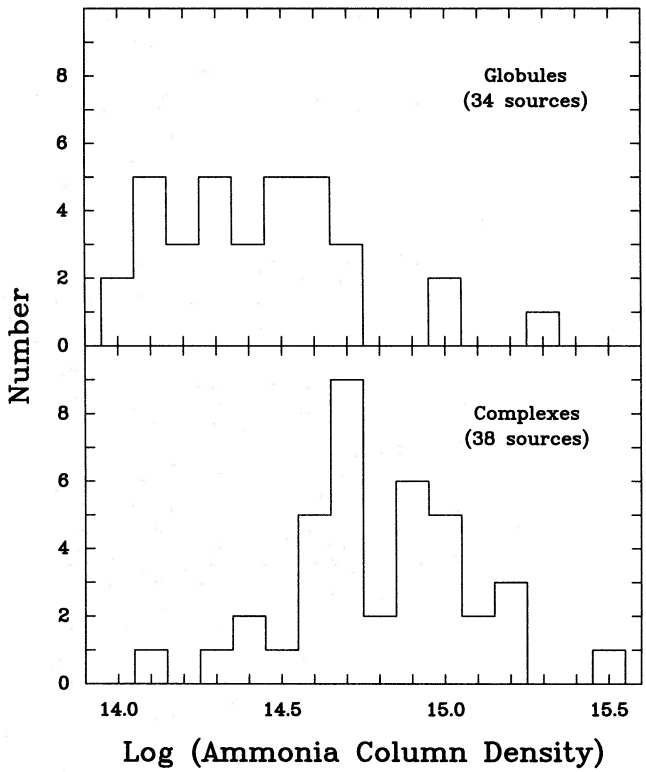

Figure 4. Histograms of the total ammonia column density, $N(NH_3)$, in cm^{-2}, for globules (upper) and cores within complexes (lower).

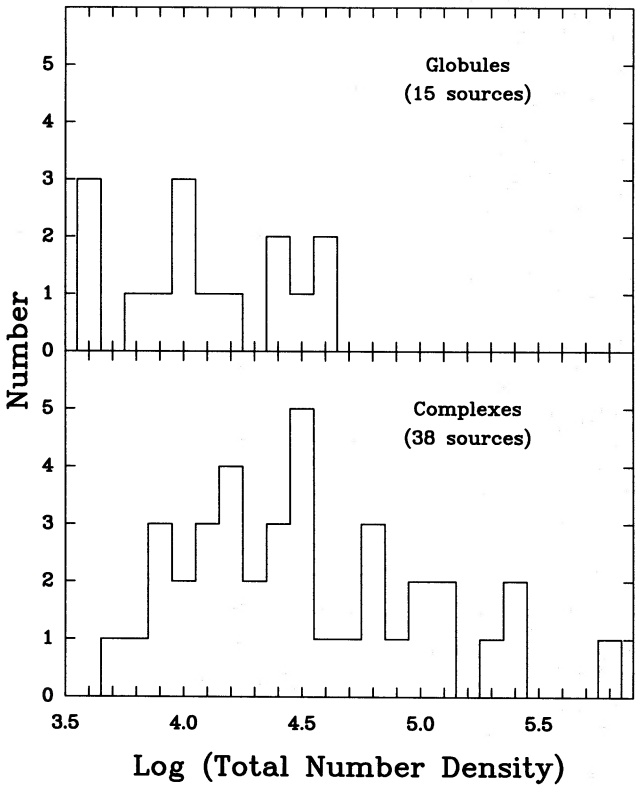

Figure 5. Histograms of the total number density, $n(H_2)$, in cm^{-3}, for globules (upper) and cores within complexes (lower).

same parent distribution is less than 1 per cent. When applying the test to the opacity data, the same result is found.

An attempt has been made to eliminate biases due to distance effects in the above comparisons by removing the Taurus and Ophiuchus cores from the BM sample. However, the possibility that the effect of beam dilution is masking the true nature of the globules cannot be ruled out altogether, since BM showed that, if they move their Taurus sources to a distance of 420 pc, only three of that sample remain as strong detections. We believe, however, that the difference observed between the globules and complexes may be real, and due primarily to the different environments in which they reside.

Finally, Table 6 shows that the sizes of the cores in both samples are very nearly equal, with a mean value of ~0.2 pc. As a result the cores in complexes are, on the average, more massive than the cores within globules, as shown in Table 6.

5.2 Globule sizes

It was suggested in Section 5.1 that some globules may not have been detected in ammonia because of their size. If they are small compared with the Parkes beamsize at 23.7 GHz of 1.4 arcmin, they will suffer from beam dilution effects. If, on the other hand, they are large, we may not have observed the densest part of the globule. We will now look at the cloud sizes and the number of detections for each cloud size to see if there is any evidence to support this conjecture. Table 7 shows the number of clouds detected in each size range. Column 1 lists the size ranges, column 2 the number of detections in each size range, column 3 the number of non-detections in each size range, and column 4 the number of detections as a percentage of the total number of clouds in each size range.

Table 7. The number of clouds in this survey detected in each size range is shown. The size is the geometric mean size as shown in table 1 of Paper 1.

Size Range	Detections	Non-detections	% Detected
$< 1'$	1	2	33
$1 - 2'$	13	23	36
$2 - 3'$	31	25	55
$3 - 4'$	21	13	62
$4 - 5'$	9	8	53
$> 5'$	9	14	39

It can immediately be seen that the smaller globules (<2 arcmin) are not readily detected (detection rate 36 per cent). As suggested above, beam dilution is the likely reason, because of their apparent small size, as a result of their being either more distant or intrinsically small. However, we also see a relatively low detection rate for the largest globules (>5 arcmin) of 39 per cent. Again, a likely reason has already been suggested. It is quite possible that with the large globules we have not observed the densest part of the globule, which is difficult to determine by eye when the globule extends more than a few arcminutes. In general only one position within each globule has been searched, so more positions in these globules should be searched for ammonia emission. It seems unlikely that many of the largest undetected globules will become strong ammonia detections, unless their core size is very small. However, BM found that many of the positions that they initially surveyed showed weak or no emission, although subsequent searches around these positions revealed the ammonia cores (P. J. Benson, private communication).

5.3 Cometary globules

The cometary globules (CGs) associated with the Gum nebula in Vela (Hawarden & Brand 1976; Sandqvist 1977; Reipurth 1983; Zealey et al. 1983) form an interesting subsample of the list of globules presented here. The favoured scenario for their formation has been discussed by Reipurth (1983). They appear to have been subjected to a considerable external pressure in the form of a stellar wind from the extremely luminous O4 star ζ Puppis (Reipurth 1983), which may have resulted in significant compression of their heads. Did they exist as cores within a larger cloud complex before they were disrupted, or were the cores formed by the passage of the wind? The situation in Vela appears to be unique, as very few CGs are seen elsewhere in the sky.

In this study there are 32 globules that have been identified as possibly associated with the Gum nebula region (Reipurth 1983; Zealey et al. 1983), which we have observed for ammonia emission. We have also observed four of the globular dark clouds (GDCs) in Vela identified by Reipurth (1983), these being GDC1 (DC 267.4−7.5), GDC2 (DC

267.5 − 7.4), GDC4 (DC 267.2 − 7.2) and GDC5 (DC 267.7 − 7.4). Of this list of 36, four are found to be strong emitters of ammonia (11 per cent), and 23 have detections greater than 3σ (64 per cent). We thus find that as a group the CGs are detected more frequently than the other Bok globules in this study (75 per cent compared with only 38 per cent). Such a high detection rate would suggest that the external forces which have been at work on the CGs have had a significant effect on their internal structure. Of the nine CGs with geometric head sizes ≤ 1 arcmin, seven were not detected in ammonia, while the two that were had the lowest antenna temperatures amongst the CGs. If beam dilution is the reason for their non-detections, then it may be that all the CGs in the Vela region contain dense cores. At an assumed distance of 400 pc, the CGs with head sizes ≤ 1 arcmin have beam filling factors < 0.35, so beam dilution is important; however, such cores may simply not be massive enough to be detected at this distance.

Four of the globules have been mapped in sufficient detail for their core sizes to be derived. For three of these the core size closely approximates the optical size of the globule head. Table 8 shows the properties derived for the CGs based on the assumptions outlined below. Column 1 lists the cloud number, column 2 the CG name, as given by Zealey et al. (1983) and Reipurth (1983), and column 3 the corrected antenna temperature. Column 4 lists the optical head size in arcminutes, column 5 the beam filling factor, and column 6 the core diameter in parsecs, assuming a common distance of 400 pc to the CGs. Column 7 lists the (1,1) column density, column 8 the total ammonia column density, and column 9 the molecular hydrogen density. Column 10 indicates the approximate core mass, and column 11 the estimated bolometric luminosity of any associated *IRAS* sources.

The core size is assumed to equal the optical size of the CG head for the reason given above (except for GDC5, which we have mapped and which has a core size less than the head size). This is probably an overestimate in many cases, but it is the best approximation at which we can arrive, and will not have a significant affect on our conclusions. For positions where it has not been possible to fit model NH_3

Table 8. Derived properties of cometary globules in the Vela–Gum nebula region.

Number	Name	T_a^* (K)	$a \times b^{(a)}$	ϕ	d (pc)	$N(1,1)^{(b)}$ ($\times 10^{13}$ cm^{-2})	$N(NH_3)$ ($\times 10^{14}$ cm^{-2})	$n(H_2)^{(c)}$ ($\times 10^3$ cm^{-3})	M ($M_\odot$)	L_{bol} ($L_\odot$)
17	CG1	0.10	2′ × 2′	0.67	0.23	3.6*	1.1	2.6	1.1	17
15	CG2	0.11	2′ × 2′	0.67	0.23	2.3†	0.7	1.6	0.7	1.9
25	CG3	0.17	3′ × 1.5′	0.66	0.25	5.9*	1.8	4.0	2.0	2.8
21	CG4	0.20	4′ × 1′	0.55	0.23	3.7†	1.1	2.6	1.1	
19	CG5	0.09	1′ × 0.5′	0.20	0.08	5.2†	1.6	10.5	0.2	1.3
20	CG6	0.19	3′ × 1′	0.53	0.20	4.8†	1.5	4.0	1.1	
32	CG7	...	2′ × 1.5′	0.60	0.20					
169	CG11	...	2.5′ × 1.5′	0.64	0.23					
92	CG12	0.11	4′ × 3′	0.86	0.40	3.5†	1.1	1.5	3.2	56
22	CG13	0.12	5′ × 3′	0.87	0.45	1.8†	0.6	0.7	2.0	
26	CG14	0.11	3′ × 1′	0.53	0.20	2.6†	0.8	2.2	0.6	1.9
27	CG15	0.19	3′ × 1′	0.53	0.20	3.6†	1.1	3.0	0.8	1.1
28	CG16	0.21	2′ × 1′	0.48	0.16	10.4	3.2	10.5	1.6	
46	CG17	...	1′ × 1′	0.34	0.12					
45	CG18	...	0.5′ × 0.5′	0.11	0.06					
83	CG19	0.12	2′ × 1′	0.48	0.16	5.8*	1.8	5.9	0.9	2.7
82	CG20	0.19	4′ × 1.5′	0.69	0.29	2.8†	0.9	1.6	1.3	
80	CG21	...	7′ × 2′	0.80	0.44					
13	CG22	0.14	5′ × 3′	0.87	0.45	3.5*	1.1	1.3	3.9	3.7
24	CG24	0.07	1′ × 1′	0.34	0.12	2.4†	0.8	3.5	0.2	
5	CG26	0.23	2′ × 1′	0.48	0.16	6.8*	2.1	6.8	1.0	0.9
2	CG27	0.22	2′ × 1′	0.48	0.16	5.0†	1.6	5.1	0.8	1.1
3	CG28	...	1′ × 1′	0.34	0.12					1.3
4	CG29	...	1′ × 1′	0.34	0.12					
12	CG30	0.64	3′ × 2′	0.74	0.29	16.1	5.0	9.4	7.2	13
8	CG31A	0.35	4′ × 2′	0.77	0.33	7.2*	2.2	3.6	4.3	
9	CG31B	0.19	2′ × 2′	0.67	0.23	3.4*	1.0	2.4	1.0	
10	CG31C	0.24	3′ × 2′	0.74	0.29	5.4*	1.7	3.2	2.4	
11	CG31D	...	1′ × 1′	0.34	0.12					
7	CG32	0.22	3′ × 1.5′	0.66	0.25	11.8	3.6	8.0	4.0	9.2
6	CG33	...	0.8′ × 0.6′	0.20	0.08					
14	CG34	0.24	3′ × 1′	0.53	0.20	9.4	2.9	7.8	2.1	
18	CG36	...	1′ × 1′	0.34	0.12					1.3
36	GDC1	0.39	4′ × 3′	0.86	0.40	9.7	3.0	4.0	8.7	18
37	GDC2	0.30	2′ × 2′	0.67	0.23	9.9	3.1	7.1	3.0	
34	GDC4	0.20	2′ × 2′	0.67	0.23	3.6*	1.1	2.6	1.1	3.3
41	GDC5	0.75	2.4′ × 1.9′	0.67	0.23	19.8	6.1	14.3	5.8	4.4

Notes. [a]Optical head size, except for GDC5 (see text).
[b]* indicates that $N(1, 1)$ is determined from integrating over the satellite lines; † indicates that $N(1, 1)$ is determined from integrating over the main-line group.
[c]Ammonia abundance of 3×10^{-8} assumed.

spectra, the cloud average for T_{ex} of 6 K has been assumed, again probably an overestimate in many cases. An attempt has been made to determine the lower limit to the (1,1) column density using one of the methods outlined in Section 3.1.2, either by fitting the ammonia hyperfine pattern to the observed spectra, or by integrating over the spectral lines and assuming optically thin conditions. For four of the CGs it has been possible to determine the kinetic temperature. For two of the 'true' CGs in the list (CG30 and CG31A), $T_R \sim T_K \sim 13$ K, while for the other two (GDC1 and 5) the values of T_R are 16 and 11 K respectively. Thus a value for the kinetic temperature of 13 K has been assumed for the cometary globules. The CGs appear slightly warmer than the average core as defined by the work of BM ($T_K \sim 10$ K), although the temperatures of a larger number of CGs need to be determined to state this with certainty [Harju et al. (1990) find $T_K = 15$ K for the core region of CG1, and González-Alfonso, Cernicharo & Radford (1995) find $T_K \sim 16$ K for CG4 and CG6]. With these assumptions we are able to estimate the total column densities of NH_3 for the detected CGs from equation (10) and, assuming a value for the ammonia abundance, lower limits to their densities from equation (12).

For the globule sample as a whole, we find a median value for the ammonia abundance of 3×10^{-8} (10 sources) where we have been able to determine it, which is similar to that found by Harju et al. (1993). The abundance is thus assumed to be 3×10^{-8} in the calculations here. The masses may then be estimated by adopting a distance of 400 pc to the CGs. The luminosities of any associated *IRAS* sources may also be estimated as outlined in Section 5.4 below. The flux quality of the *IRAS* associations has been ignored when selecting sources possibly associated with the CGs. By comparing the occurrence of *IRAS* sources lying toward the CGs with that of the surrounding sky, Bhatt (1993) has shown that the *IRAS* sources found lying within the Vela CG optical boundaries have a high probability of being true associations.

The derived average value for the ammonia column density of the CGs is $N(NH_3) = (1.9 \pm 1.3) \times 10^{14}$ cm^{-2}, while the mean hydrogen number density is $n(H_2) = (5 \pm 3) \times 10^3$ cm^{-3}. The uncertainties quoted here are the standard deviations of the distributions and are intended to give an idea of the range of values observed. The assumptions that we have made suggest that these values are probably lower limits in most cases. Thus a 'typical' CG in the Vela region has an ammonia column density $N(NH_3) \sim (2\text{–}3) \times 10^{14}$ cm^{-2} and a density $n(H_2) \sim (5\text{–}8) \times 10^3$ cm^{-3}, similar to those of the other globules and therefore also lower than those of the cores within complexes. The core mass is typically a few $M_\odot$. For the associated *IRAS* sources, we find a median value for the bolometric luminosity of $\sim 3 L_\odot$.

Recently, Vilas-Boas, Myers & Fuller (1994, hereafter VMF) have surveyed a number of the Vela CGs with the Swedish-European Southern Observatory Submillimetre Telescope (SEST) for CO emission. For CGs appearing in both surveys, the physical properties have been determined for 17 sources by VMF, and for 16 sources in this study. Of the 16 common sources detected by both groups, properties have been derived by both groups for 13. In order to determine the CG properties, VMF have made a number of assumptions, most of which differ from those used in this section, as a result of the different natures of the molecules observed.

The column density, $N(H_2)$ determined by VMF is $(5.1 \pm 0.4) \times 10^{21}$ cm^{-2} for the 17 sources, while in the present work the derived value is $(6.5 \pm 1.0) \times 10^{21}$ cm^{-2} [using the values of $N(NH_3)$ from Table 8 and an ammonia abundance of 3×10^{-8}]. For the hydrogen number density, $n(H_2)$, the values are $(5.6 \pm 0.7) \times 10^3$ cm^{-3} for VMF and $(5.2 \pm 0.8) \times 10^3$ cm^{-3} for this work. VMF state that their values are upper limits, while we believe that our values are lower limits in most cases. While it is difficult to compare the two sets of results directly, the joint results suggest that $N(H_2) \sim 6 \times 10^{21}$ cm^{-2} and $n(H_2) \sim 5 \times 10^3$ cm^{-3} are typical values for the opaque heads of the Vela CGs.

For the 22 Vela CG sources detected in ^{13}CO by VMF, the velocity dispersion (standard deviation of the observed radial velocities) is 4.6 km s^{-1}, while for 27 sources detected here the velocity dispersion is slightly larger at 5.5 km s^{-1}. For the 16 common sources detected by both groups, we find that there exists a systematic offset in the observed velocities of ΔV_{lsr} ($^{13}CO - NH_3$) = 0.26 km s^{-1}, with a standard deviation of 0.14 km s^{-1}. A comparison of the velocities determined for CG4 and CG6 in this study and by VMF with those determined by González-Alfonso et al. (1995) (using SEST) suggests that the source of the systematic offset lies with VMF. The (0,0) positions observed by González-Alfonso et al. (1995) are very similar to the positions observed by VMF and in the present study. For CG4, González-Alfonso et al. (1995) determine V_{lsr} ($C^{18}O$) = 1.5 km s^{-1}, compared with 1.45 km s^{-1} for this work and 1.82 km s^{-1} for VMF. For CG6, the corresponding velocities are 1.0, 0.93 and 1.16 km s^{-1}. In addition using $C^{18}O$, VMF determined $V_{lsr} = 1.15$ km s^{-1} for CG6, in accord with their value for ^{13}CO.

BM showed that, if their Taurus cores were moved to a distance of 420 pc, only three of their 13 strong detections would remain strong, compared with four for CGs at a similar distance. This supports the claim that the values derived here are lower limits, as a result in part of beam dilution. As shown in the following section, 48 per cent of the CGs with ammonia detections have an associated *IRAS* source, compared with only 29 per cent for the other globules surveyed here. The large number of *IRAS* sources associated with the CGs, and the large percentage of ammonia detections, suggests that star formation in CGs is enhanced compared with other Bok globules. This argues against the idea that all isolated Bok globules have passed through a CG phase in their evolution, although it certainly does not rule out the possibility that the CGs will eventually form isolated globules. The parameters derived here for the CGs indicate that only low-mass star formation is occurring within them. All indications are that the event responsible for the formation of the CGs has triggered a burst of star formation within them, and reinforces the argument that the dense core's environment plays a major role in determining its evolution.

5.4 *IRAS* sources in globules and complexes

The *IRAS* sources associated with the dark clouds in this work are listed in table 2 of Paper I. All *IRAS* sources that lie within the cloud boundaries are shown in this table, regardless of the quality of their detections. It was noted in Paper I that, if the *IRAS* flux sensitivity limits could be reduced from

3 to 1 Jy, almost all globules would be detected at 100 μm, a result which was first shown by Clemens et al. (1991).

More stringent selection criteria will now be applied to the *IRAS* sources, in an attempt to identify true point sources associated with the globules. In order to compare the number of sources associated with globules with those found in the cores in complexes, the selection criteria of BM are used. To be included here the *IRAS* sources must have been detected in at least two of the four *IRAS* wavebands, with a greater flux density at the longer wavelength. A total of 40 sources in 39 globules satisfy these criteria, while BM found 39 sources in 28 cores. The sources satisfying these criteria are shown in Table 9. Column 1 lists the cloud number, column 2 the cloud name, column 3 the *IRAS* name and column 4 the adopted distance. The distance estimates are derived from stellar reddening as described earlier, unless otherwise noted. Columns 5–7 list the derived luminosities. The bolometric luminosity, $L_{\rm bol}$, may be estimated from $L_{\rm bol} = L_{IRAS} + \Delta L$, where L_{IRAS} is obtained from (Parker 1991)

$$L_{IRAS} = 4\pi D^2 \int_{12\ \mu\mathrm{m}}^{100\ \mu\mathrm{m}} S_\lambda \, \mathrm{d}\lambda$$

$$\simeq 4.7 \times 10^{-6} D^2 \left(\frac{S_{12}}{0.79} + \frac{S_{25}}{2} + \frac{S_{60}}{3.9} + \frac{S_{100}}{9.9} \right) \mathrm{L}_\odot; \qquad (15)$$

Table 9. *IRAS* sources associated with small southern dark clouds satisfying the selection criteria of BM.

Number	DC Name	*IRAS* Name	$D^{(a)}$ (pc)	L_{IRAS} ($L_\odot$)	ΔL ($L_\odot$)	L_{bol} ($L_\odot$)
15	255.3–14.4	07144–4352	400[1]	1.1	0.8	1.9
17	256.2–14.1	07178–4429	400[1]	14	2.9	17
26	262.5–13.4	07372–4945	400[1]	1.1	0.8	1.9
25	260.7–12.4	07378–4745	400[1]	1.7	1.1	2.8
19	257.2–10.3	07391–4342	400[1]	0.9	0.4	1.3
12	253.3–1.6	08076–3556	400[1]	9.1	4.1	13
7	252.5+0.1	08124–3422	400[1]	5.7	3.5	9.2
36	267.4–7.5	08242–5050	400[1]	13	5.0	18
34	267.2–7.2	08250–5030	400[1]	1.9	1.5	3.3
41	267.7–7.4	08261–5100	400[1]	3.5	0.9	4.4
13	253.6+2.9	08267–3336	400[1]	2.5	1.2	3.7
23	259.9–0.0	08337–4028	500	279	169	448
23	259.9–0.0	08337–4024	500	6.1	4.7	11
18	256.9+2.6	08354–3926	400[1]	0.9	0.5	1.3
55	275.9+1.9	09449–5052	300	2.0	1.1	3.1
58	289.3–2.8	10471–6206	250	1.6	1.2	2.9
71	297.7–2.8	11590–6452	175[2]	6.1	3.1	9.2
79	301.7–6.7	12345–6910	175[2]	0.7	0.3	1.0
83	302.1+7.4	12427–5508	300	0.9	0.6	1.5
86	303.8–14.2	13036–7644	200[3]	0.9	0.5	1.4
87	307.3+2.9	13224–5928	400	6.4	3.2	9.6
92	316.5+21.2	13547–3944	400[1]	39	17	56
88	314.8–5.1	14451–6502	400	4.4	1.9	6.3
101	320.7–1.7	15148–5911	350	10	8.1	18
100	320.5–3.6	15215–6056	350	1.8	1.1	2.9
98	320.1–4.3	15223–6146	350	1.2	0.8	2.0
136	344.5+2.0	16510–4026	350	6.8	3.7	11
121	337.1–4.9	16554–5031	300	2.7	2.3	5.0
154	351.2+5.2	16590–3313	700	6.9	2.3	9.2
153	351.2+5.1	16594–3315	700	14	2.6	17
148	349.0+3.0	17011–3613	200	1.0	0.8	1.8
149	349.2+3.1A	17012–3603	200	1.0	0.7	1.7
167	354.2+3.2	17151–3202	200	1.8	0.9	2.8
160	353.3+2.4	17156–3312	200	2.6	1.5	4.2
164	354.1+2.9C	17157–3212	200	2.2	0.9	3.1
159	353.1+2.3	17159–3324	200	6.6	5.9	13
139	345.2–3.6	17172–4316	400	3.7	2.5	6.2
137	344.6–4.3	17181–4405	700	87	44	131
140	345.4–4.0	17193–4319	400	3.2	2.0	5.1
168	356.5–4.5	17518–3414	300	1.1	0.8	1.9

Notes.
[a][1]Vela CG; [2]proximity to Coalsack; [3]proximity to Chamaeleon II; others from reddening.

where, D is the source distance in parsecs and S_λ the flux density in Jy at wavelength λ.

Since the flux is increasing with wavelength, a significant fraction of the flux may be emitted at wavelengths longer than 100 μm. The bolometric correction to the luminosity for these wavelengths may be estimated from

$$\Delta L = 5.33 \times 10^{-5} D^2 \left(\frac{S_{100}}{100}\right) \mathrm{L}_\odot, \qquad (16)$$

assuming that the maximum flux density over the entire spectrum occurs at 100 μm, and that the spectrum is a blackbody for wavelengths greater than 100 μm (Myers et al. 1987). Although the wavelength dependence of the dust grain emissivity probably varies as λ^{-1} or λ^{-2} beyond 100 μm, the range of grain temperatures present will broaden the distribution by some unknown amount. Thus the assumption of a blackbody spectrum in the far-infrared beyond 100 μm is not unreasonable. No correction has been made for the luminosity at wavelengths shorter than 12 μm. The mean bolometric luminosity of the sources in Table 9 with $L_{\rm bol} < 50\,\mathrm{L}_\odot$ (37 sources) is $6.2 \pm 0.9\,\mathrm{L}_\odot$. For the BM sample the mean bolometric luminosity is $2.6 \pm 0.6\,\mathrm{L}_\odot$ (37 sources with $L_{\rm bol} < 50\,\mathrm{L}_\odot$, after one of the two L1495N sources with identical fluxes has been removed). Both samples therefore consist primarily of low-luminosity, low-mass sources. Note that, of the three sources we have excluded from our average, two are associated with bright reflection nebulosities [DC 259.9 − 0.0 (BHR 23) and DC 316.5 + 21.2 (BHR 92)], while the other [DC 344.6 − 4.3 (BHR 137)] contains a near-infrared reflection nebulosity associated with the embedded source, as indicated by our unpublished near-infrared observations.

For this work we find that 7 of the 10 strong sources (70 per cent) have an associated *IRAS* source, while BM found 27 sources in their 40 nearby ($D < 500$ pc) strong detections (68 per cent), so the results are similar. Strong ammonia emission would seem to be a good indicator of low-mass star formation, as suggested by BM, regardless of the core type. For the moderate detections, only 20 of our 66 cores have an associated *IRAS* source (30 per cent), while, for the cores in complexes, BM found that 9 of 19 moderate detections have an *IRAS* source (47 per cent). So, for good ammonia detections ($> 3\sigma$), only 27 of 76 (36 per cent) are associated with an *IRAS* point source, implying that, for globules alone, detection of ammonia is only a moderately good indicator of an advanced low-mass star formation site. For cores in complexes the opposite conjecture appears valid, since 36 of 59 (61 per cent) nearby cores with good ammonia detections have an associated *IRAS* source. This result, combined with the findings of Section 5.1, indicates that, while low-mass star formation is occurring in some globules (see e.g. Yun & Clemens 1990; Bourke et al. 1993), the efficiency of star formation appears lower than that for cores within larger dark cloud complexes. Of the 76 ammonia detections of globules, 27 are of Vela CGs, of which 13 (48 per cent) have an associated *IRAS* source satisfying the BM criteria, compared with only 14 of the 49 other globules (29 per cent) detected.

6 SUMMARY AND CONCLUSIONS

The catalogue of small, isolated molecular clouds (globules) presented in Paper I has been surveyed with the Parkes radio telescope for emission in the (1,1) inversion transition of ammonia. Approximately half of the 169 clouds surveyed were detected, with 6 per cent of these detections being strong. This result indicates that approximately half of the globules have densities sufficient to suggest that they may be gravitationally bound, with some undergoing contraction leading to star formation.

The principal conclusions of this work are as follows.

(i) The cores within globules are found to be less opaque and less dense than those found within complexes. The strength of the ammonia emission from the globules is on average less than that observed from the cores within complexes, with only 6 per cent of the globules being strong detections, while ~25 per cent of the cores within complexes are found to be strong. This may be a direct result of the globules being less opaque and less dense than the cores within complexes. The average values of the other properties of the cores within the globules, such as temperature, core sizes, and luminosity of associated *IRAS* sources, are similar to those of the cores within complexes, while their masses are lower.

(ii) Small globules (< 2 arcmin) are not as readily detected in ammonia emission as the larger globules, probably due to beam dilution, since the beamsize used was 1.4 arcmin. Clearly, high-resolution observations of these globules with a high-density gas tracer are required. Large globules (5–10 arcmin) are also not readily detected. The reason for this is not clear, but may be due to cores being missed by the telescope beam, since in general only one position within each cloud was searched. These large globules should be searched in more detail for possible missed cores.

(iii) The Vela-Gum nebula cometary globules, as a subsample of the globules surveyed, are detected in ammonia emission in a significantly higher percentage than the other globules surveyed (75 compared with 38 per cent), and appear to be more active sites of star formation. We suggest that this is a consequence of their environment, in particular the presence of a significant stellar wind. Furthermore, the enhanced star formation in CGs, combined with their rare occurrence, renders it most unlikely that all Bok globules have passed through a CG phase in their evolution, although some of them most certainly have. The properties of the CGs are similar to those of the other globules, with densities of $\sim 5 \times 10^3\ \mathrm{cm}^{-3}$, core masses of a few $\mathrm{M}_\odot$, and *IRAS* sources with luminosities of a few $\mathrm{L}_\odot$.

(iv) *IRAS* sources that satisfy the BM selection criteria are associated with a lower percentage of the cores in globules (as defined by the detection of ammonia) than are such *IRAS* sources that are associated with the cores within complexes (36 per cent compared with 61 per cent). This may imply that the detection of ammonia toward a globule is only a moderate indicator of a site of low-mass star formation, unless the detection is strong.

Thus, by combining the results that cores in complexes are denser than the isolated globules, and that the cores in complexes and the CGs are more active sites of star formation than isolated globules, it becomes clear that the environment in which the core resides, in particular the presence of either a large external mass or a stellar wind, plays a significant role in the general process of initiating low-mass star formation.

ACKNOWLEDGMENTS

First, we acknowledge the Australia Telescope National Facility (ATNF) for the most generous allocation of time on the Parkes radio telescope. Many people assisted with the observations at the telescope, and we particularly thank Simon Duchesne, Chris Lidman, Peter McGregor, Craig Smith, Robert Smith, Liam Waldron and Andrew Walsh, as well as the entire staff of the Parkes Observatory. Drs John Whiteoak and Rick Forster were always most willing to provide expert guidance with the reduction of the ammonia observations. Henrietta May of the ATNF was of great assistance with the ATNF spectral line reduction package SPC. We acknowledge the many suggestions of the referee, Dr D. P. Clemens, which we believe have led to a significant improvement in this paper. The assistance of Mt Stromlo and Siding Spring Observatories in allowing us access to their Schmidt plates and computing facilities is also gratefully acknowledged. This project has been supported in part by a grant from the Australian Research Council. One of us (TLB) thanks the Department of Physics, University College, for financial assistance during part of this study.

REFERENCES

Bachiller R., Guilloteau S., Kahane C., 1987, A&A, 173, 324
Benson P. J., 1983, PhD thesis, Massachusetts Institute of Technology
Benson P. J., Myers P. C., 1989, ApJS, 71, 89 (BM)
Bevington P. R., 1969, Data Reduction and Error Analysis for the Physical Sciences. McGraw-Hill, New York
Bhatt H. C., 1993, MNRAS, 262, 812
Bok B. J., 1977, PASP, 89, 597
Bok B. J., Reilly E. F., 1947, ApJ, 105, 255
Bourke T. L., 1994, MSc thesis, University of New South Wales
Bourke T. L., Hyland A. R., Robinson G., James S. D., 1993, Proc. Astron. Soc. Aust., 10, 236
Bourke T. L., Hyland A. R., Robinson G., 1995, MNRAS, 276, 1052 (Paper I, this issue; BHR)
Clemens D. P., Barvainis R., 1988, ApJS, 68, 257
Clemens D. P., Yun J. L., Heyer M. H., 1991, ApJS, 75, 877
Danby G., Flower D. R., Valiron P., Schilke P., Walmsley C. M., 1988, MNRAS, 235, 229
de Vries C. P., Brand J., Israel F. P., de Graauw Th., Wouterloot J. G. A., van de Stadt H., Habing H. J., 1984, A&AS, 56, 333
Dickman R. L., Clemens D. P., 1983, ApJ, 271, 143
Genzel R., 1991, in Pfenniger D., Bartholdi P., eds, The Galactic Interstellar Medium. Springer-Verlag, Berlin, p. 275
González-Alfonso E., Cernicharo J., Radford S. J. E., 1995, A&A, 293, 493
Goss W. M., Manchester R. N., Brooks J. W., Sinclair M. W., Manefield G. A., Danzinger I. J., 1980, MNRAS, 191, 533
Harju J., Sahu M., Henkel C., Wilson T. L., Sahu K. C., Pottasch S. R., 1990, A&A, 233, 197
Harju J., Walmsley C. M., Wouterloot J. G. A., 1993, A&AS, 98, 51
Hawarden T. G., Brand P. W. J. L., 1976, MNRAS, 175, 19P
Herbst W., 1977, PASP, 89, 795
Ho P. T. P., Townes C. H., 1983, ARA&A, 21, 239
Hughes J., Hartigan P., 1992, AJ, 104, 680
Kuiper T. B. H., Peters W. L., III, Forster J. R., Gardner F. F., Whiteoak J. B., 1987, PASP, 99, 107
Lynds B. T., 1968, in Middlehurst B. M., Aller L. H., eds, Nebulae and Interstellar Matter. Univ. Chicago Press, Chicago, p. 119
Martin R. N., Barrett A. H., 1978, ApJS, 36, 1
Morris-Kennedy P., 1983, MK Classification Extension. Mt Stromlo Obs., Canberra (also in The Astronomical Data Centre CD-ROM Selected Astronomical Catalogs, Vol. 1, 1989)
Myers P. C., 1983, ApJ, 270, 105
Myers P. C., 1985, in Peimbert M., Jugaku J., eds, IAU Symp. 115, Star Forming Regions. Reidel, Dordrecht, p. 33
Myers P. C., Fuller G. A., Matthieu R. D., Beichamn C. A., Benson P. J., Schild R. E., Emerson J. P., 1987, ApJ, 319, 340
Parker N. D., 1991, MNRAS, 251, 63
Pauls T. A., Wilson T. L., Bieging J. H., Martin R. N., 1983, A&A, 124, 23
Reipurth B., 1983, A&A, 117, 183
Rieke G. H., Lebofsky M. J., 1985, ApJ, 288, 618
Rodgers A. W., 1960, MNRAS, 120, 163
Sandqvist Aa., 1977, A&A, 57, 467
Sandqvist Aa., Lindros K. P., 1976, A&A, 53, 179
Snell R. L., 1981, ApJS, 45, 121
Stutzki J., Winnewisser G., A&A, 144, 13
Stutzki J., Jackson J. M., Olberg M., Barrett A. H., Winnewisser G., 1984, A&A, 139, 258
Turner B. E., 1993, ApJ, 411, 219
Ungerechts H., Walmsley C. M., Winnewisser G., 1980, A&A, 88, 259
Vilas-Boas J. W. S., Myers P. C., Fuller G. A., 1994, ApJ, 433, 96 (VMF)
Walmsley C. M., Ungerechts H., 1983, A&A, 122, 164
Yun J. L., Clemens D. P., 1990, ApJ, 367, L73
Zealey W. J., Ninkov Z., Rice E., Hartley M., Tritton S. B., 1983, Astrophys. Lett., 23, 119